Molecular Biology of the Cell
Vol. 7, 631–650, April 1996

Golgi Dispersal during Microtubule Disruption: Regeneration of Golgi Stacks at Peripheral Endoplasmic Reticulum Exit Sites

Nelson B. Cole, Noah Sciaky†, Alex Marotta, Jia Song, and Jennifer Lippincott-Schwartz*

Cell Biology and Metabolism Branch, National Institute of Child Health and Human Development, National Institutes of Health, Bethesda, Maryland 20892

Submitted October 5, 1995; Accepted January 17, 1996
Monitoring Editor: Ari Helenius

Microtubule disruption has dramatic effects on the normal centrosomal localization of the Golgi complex, with Golgi elements remaining as competent functional units but undergoing a reversible "fragmentation" and dispersal throughout the cytoplasm. In this study we have analyzed this process using digital fluorescence image processing microscopy combined with biochemical and ultrastructural approaches. After microtubule depolymerization, Golgi membrane components were found to redistribute to a distinct number of peripheral sites that were not randomly distributed, but corresponded to sites of protein exit from the ER. Whereas Golgi enzymes redistributed gradually over several hours to these peripheral sites, ERGIC-53 (a protein which constitutively cycles between the ER and Golgi) redistributed rapidly (within 15 minutes) to these sites after first moving through the ER. Prior to this redistribution, Golgi enzyme processing of proteins exported from the ER was inhibited and only returned to normal levels after Golgi enzymes redistributed to peripheral ER exit sites where Golgi stacks were regenerated. Experiments examining the effects of microtubule disruption on the membrane pathways connecting the ER and Golgi suggested their potential role in the dispersal process. Whereas clustering of peripheral pre-Golgi elements into the centrosomal region failed to occur after microtubule disruption, Golgi-to-ER membrane recycling was only slightly inhibited. Moreover, conditions that impeded Golgi-to-ER recycling completely blocked Golgi fragmentation. Based on these findings we propose that a slow but constitutive flux of Golgi resident proteins through the same ER/Golgi cycling pathways as ERGIC-53 underlies Golgi dispersal upon microtubule depolymerization. Both ERGIC-53 and Golgi proteins would accumulate at peripheral ER exit sites due to failure of membranes at these sites to cluster into the centrosomal region. Regeneration of Golgi stacks at these peripheral sites would re-establish secretory flow from the ER into the Golgi complex and result in Golgi dispersal.

INTRODUCTION

The nature and function of the Golgi apparatus has attracted a great deal of attention among cell biologists for many years (Farquhar and Palade, 1981; Mellman and Simons, 1992; Rothman and Orci, 1992). This is due not only to the Golgi's central role in membrane traffic and sorting within the secretory pathway, but also to its unique structure, distribution, and dynamics within cells. The Golgi complex in nonpolarized cells is usually localized to the centrosomal region and consists of interconnected, polarized stacks of flattened cisternae enriched in glycoprotein and glyco-

* Corresponding author: Cell Biology and Metabolism Branch, NICHD, NIH Building 18T, Room 101, Bethesda, MD 20892.
† Current address: National Jewish Center for Immunology and Respiratory Medicine, 1400 Jackson St., Denver, CO 80206.

lipid processing enzymes (Beams and Kessel, 1968; Rambourg and Clermont, 1990). Specialized sorting and transport machinery enable the Golgi to filter selected membrane and protein components from secretory bulk flow derived from the endoplasmic reticulum (ER) (Pryer *et al.*, 1992; Rothman, 1994). Because many of the components of this machinery must be retrieved back to the ER for continued use, significant exchange of membrane occurs between the Golgi complex and the ER (Pelham, 1991). Despite its distinctive morphology, localization, and function within cells, the Golgi complex is capable of rapid disassembly and reassembly during mitosis (Lucocq *et al.*, 1987; Warren, 1993), as well as under pharmacologically induced conditions (e.g. brefeldin A [BFA], okadaic acid, and ilimaquinone (IQ)) (Lippincott-Schwartz *et al.*, 1990; Lucocq *et al.*, 1991; Takizawa *et al.*, 1993) and reversibly redistributes to numerous peripheral sites in response to microtubule depolymerization (Pavelka and Ellinger, 1983; Rogalski and Singer, 1984; Thyberg and Moskalewski, 1985; Turner and Tartakoff, 1989). How Golgi fragmentation and dispersal during these processes is accomplished is far from being understood. In this study we analyze the process of Golgi dispersal during microtubule depolymerization with the goal of understanding how it occurs and why.

It is well known that microtubules underlie the centrosomal positioning of the Golgi complex within nonpolarized cells (Wehland *et al.*, 1983; Rogalski and Singer, 1984; Thyberg and Moskalewski, 1985) and that Golgi elements actively translocate along microtubules to reach this position (Ho *et al.*, 1989). It is also recognized that microtubules play roles in facilitating membrane traffic to and from the Golgi complex (Saraste and Svensson, 1991; Mizuno and Singer, 1994; Lippincott-Schwartz *et al.*, 1995). Secretory products leaving the Golgi complex, for example, have been shown to use microtubules to localize to specific sites on the plasma membrane (Rogalski and Singer, 1984). Moreover, Golgi localization near the microtubule-organizing center likely facilitates communication between secretory and endocytic pathways (Farquhar, 1991; Cole and Lippincott-Schwartz, 1995) and appears to centralize early secretory membrane flow, which originates from numerous ER transitional element sites scattered throughout the elaborate network of ER that fills the cytoplasm (Plutner *et al.*, 1992; Saraste and Kuismanen, 1992).

Despite roles for microtubules in the localization of Golgi elements, microtubule disruption does not always interfere with membrane flow through the secretory pathway (Rogalski *et al.*, 1984; Van De Moortele *et al.*, 1993). It does, however, have dramatic effects on Golgi morphology, with hundreds of functional Golgi islands now appearing throughout the cytoplasm (Pavelka and Ellinger, 1983; Rogalski and Singer, 1984; Thyberg and Moskalewski, 1985; Turner and Tartakoff, 1989). How this dramatic redistribution of Golgi membrane occurs without fundamentally disrupting secretory flow from the ER is unknown. A widely acknowledged mechanism for Golgi dispersal during microtubule disruption is that it results from random diffusion of Golgi elements no longer tethered together by microtubules (Rogalski and Singer, 1984). Recent biophysical studies on the properties of the cytoplasm, however, lead to the question of how random dispersal of membrane structures the size of Golgi fragments could occur throughout a cytoplasm consisting of a dense, gel-like cytoskeletal matrix (Luby-Phelps, 1994; Penman, 1995). Moreover, Golgi dispersal has been shown to be an energy-dependent and temperature-sensitive process (Turner and Tartakoff, 1989), indicating that microtubule depolymerization alone is not sufficient for Golgi dispersal. These requirements indicate more is at work during Golgi dispersal than simple diffusion.

In this paper we explore potential mechanisms of Golgi dispersal during microtubule depolymerization by examining the characteristics of the dispersal process, including where Golgi membrane redistributes within the cytoplasm and the rate at which different Golgi membrane components redistribute to these sites. We also ask whether Golgi dispersal reflects properties of normal membrane trafficking within the cell, and examine the effects of microtubule depolymerization on membrane trafficking pathways leading to and from the Golgi. Finally, we consider whether Golgi dispersal serves any role in reestablishing secretory traffic after microtubule disruption. Our results demonstrate that upon microtubule disruption Golgi membrane components gradually redistribute to peripheral sites of membrane export from the ER where functional Golgi stacks are regenerated. Before this redistribution a significant block in secretory traffic and Golgi processing occurs, which is overcome only when Golgi stacks are rebuilt in the cell periphery. We propose that a slow but constitutive flux of Golgi enzymes through pathways connecting the ER and Golgi underlies this phenomenon, with Golgi enzymes accumulating at peripheral ER exit sites as a consequence of the inability of membranes at these sites to cluster into the centrosomal region in the absence of microtubules. Reassembly of small Golgi stacks at these peripheral sites would allow secretory flow from the ER into the Golgi to continue and would explain the dispersal of Golgi elements observed during microtubule depolymerization.

MATERIALS AND METHODS

Materials and Cell Culture

Nocodazole was purchased from Sigma Chemical (St. Louis, MO) and was used at concentrations between 1 and 5 μg/ml. When added to cells at 4°C, subsequent incubation at 37°C resulted in the

depolymerization of all microtubules (detected by immunofluorescence) within 5 min of warming. BFA was purchased from Epicentre Technology (Madison, WI) and was used at 1–5 μg/ml. *N*-ethylmaleimide (NEM), monensin, 2-deoxy glucose (DOG), and cytochalasin D were all purchased from Sigma Chemical. Endoglycosidase H (endo H) was purchased from New England Biolabs (Beverly, MA). AcrylAide cross-linker and GelBond PAG film were purchased from FMC Bioproducts and used as described by the manufacturer's instructions (Rockland, ME).

NRK, HeLa, and M1 fibroblasts were grown in DMEM supplemented with 10% fetal calf serum, 2 mM glutamine, and 150 μg/ml penicillin or 2.5 μg/ml gentamicin at 37°C in 5% CO_2. Human versus rodent cell types were used in different experiments because of differences in species specificity of antibodies to the Golgi and pre-Golgi markers under study.

Antibodies

The monoclonal antibody directed against the cytoplasmic tail of vesicular stomatitis virus G protein (VSV G) P5D4, was a generous gift of Dr. A. Helenius (New Haven, CT). A monoclonal antibody that recognizes ERGIC-53 was kindly provided by Dr. H.P. Hauri (Basel, Switzerland). Rabbit polyclonal antibody directed against Golgi mannosidase II (Man II) was a kind gift of Dr. K. Moremen (Athens, GA). The monoclonal antibody against rodent Man II, 53FC3, was from Dr. B. Burke (Calgary, Canada). Rabbit polyclonal antibodies to ER resident proteins were generously provided by Dr. D. Louvard (Paris, France). Rabbit polyclonal antibody N10 against human milk galactosyltransferase (Galtf) was kindly provided by Dr. E. Berger (Basel, Switzerland). Fluorescein- and rhodamine-labeled goat anti-rabbit immunoglobulins (IgGs), and fluorescein- and rhodamine-labeled goat anti-mouse IgGs were purchased from Southern Biotechnology (Birmingham, AL).

VSV Infection

Infections with ts045 VSV were performed according to a modification of the method of Bergmann (1989). Cells were rinsed twice in DMEM without serum before adding 50–100 plague-forming units/cell of ts045 VSV for 1 h at 32°C. For immunofluorescence microscopy, cells were washed two times in serum-free DMEM to remove unadsorbed virus, and then shifted in serum-containing DMEM to 40°C for 3–4 h to maintain VSV G protein in the ER. Cells were either fixed directly or subsequently incubated at various permissive temperatures to follow VSV G protein transport through the secretory pathway.

Metabolic Labeling

Cells were grown to subconfluence in 6-well cluster dishes (Costar, Cambridge, MA), infected as above, washed two times in DMEM without serum, and then incubated in serum-containing DMEM for 2–3 h at 37°C. Cells were washed with methionine-free DMEM with 20 mM *N*-2-hydroxyethylpiperazine-*N*′-2-ethanesulfonic acid (HEPES), and incubated in this medium for 15 min at 40°C. The monolayer was pulse labeled with 50–60 μCi of trans[^{35}S]-methionine (ICN Biomedicals, Costa Mesa, CA) per well for 5–7 min. The pulse was ended by removing the labeling medium and replacing it with DMEM containing 10% fetal calf serum plus 3 mM unlabeled methionine with 20 mM HEPES (chase medium). After various chase times the chase medium was removed and 1 ml of ice-cold lysis buffer (1.0% Triton X-100 in 200 mM NaCl, 25 mM Tris-HCl, pH 7.6) containing 10 μg/ml each of leupeptin and aprotinin was added directly to the cells. Cells were scraped, pipetted into microfuge tubes, and placed on ice. Cell lysates were vortexed for 15 s, and nuclei and cell debris were pelleted by centrifugation for 10 min at 12,000 × *g*.

Immunoprecipitation and Endo H Digestion of VSV G

For each immunoprecipitation, 1–2 μl of monoclonal anti-VSV G (P5D4) were pre-incubated with Sepharose 4B beads (50 μl of a 50% suspension in phosphate-buffered saline [PBS]/0.1% bovine serum albumin) for 1 h at room temperature. The antibody-bound beads were washed with PBS/0.1% bovine serum albumin and incubated with cell lysates at 4°C for 1 h on a rotary wheel. The complexes were washed twice with 1 ml wash buffer (0.1% Triton X-100 in 200 mM NaCl, 25 mM Tris-HCl, pH 7.6). After washing the immunoprecipitates, the pellet was resuspended in 1 ml 0.1% Triton X-100 in water. The sample was split into two tubes, pelleted, and incubated with or without endo H for 2–16 h at 37°C as directed by the supplier.

SDS-PAGE, Fluorography, and Quantification

Samples were heated to 95°C for 5 min, and cooled aliquots were loaded in the wells of a 7.5% SDS-acrylamide/AcrylAide gel for electrophoresis according to the method of Laemmli (1970). Gels were fixed, and impregnated with salicylic acid for fluorography. Bands were quantitated by densitometry with ImageQuant (Molecular Dynamics, Sunnyvale, CA).

Electron Microscopy

For immunoperoxidase electron microscopy, cells grown on glass coverslips were fixed with 2% formaldehyde containing lysine and periodate (McLean and Nakane, 1974), permeabilized with saponin, and then incubated with anti-ERGIC-53 antibodies followed by horseradish peroxidase (HRP)-conjugated goat anti-mouse IgG. The cells were then washed and incubated with diaminobenzidine hydrochloride and H_2O_2, and prepared for electron microscopy, as described by Yuan *et al.*, 1987. Samples that were not immunoperoxidase labeled, were fixed in 1.5% glutaraldehyde before embedding and sectioning for electron microscopy as described by Yuan *et al.*, 1987.

Fluorescence Microscopy and Image Processing

For fluorescence labeling of cells, cells grown on glass coverslips were fixed in 2% formaldehyde in PBS for 10 min at room temperature. The coverslips were washed three times in PBS containing 10% fetal bovine serum and were then incubated in PBS serum containing antibody with 0.15% saponin for 1 h. After washing to remove unbound antibody, cells were incubated with fluorescently labeled secondary antibody for 1 h followed by washing in PBS serum. Coverslips were mounted on glass slides in Fluoromount G (Southern Biotechnology) and the cells were viewed in a Zeiss IM35 or photo-microscope equipped with barrier filters to prevent cross-over of fluorescein and rhodamine fluorescence.

Images of fixed fluorescently labeled cells that were analyzed by image processing techniques (Figures 2 and 6) were acquired using a custom made inverted wide field microscope (Yona Microscopes Eikoscope, Columbia, MD). This microscope was equipped with a Zeiss infinity corrected objective (63×, 1.3 NA), rhodamine optics (excitation [485 nm band pass] and emission [530 nm long pass] filters [fluorescence set XF32, Omega Optical, Brattleboro, VT], a dichroic filter [model XF33, Omega Optical], neutral density filters (10 and 25%), and a cooled charge-coupled device (Photometrics, Tucson, AZ) having a KAF 1400 pixel Kodak chip for 12 bit image detection. Biological Detection Systems imaging software (version 1.6, now Oncor imaging; Oncor Instruments, San Diego, CA) was used to control image acquisition on a MacIntosh Computer (Quadra 800). Images were manipulated using IPlab Spectrum (Signal Analytics, Vienna, VA) and NIH-Image software (Wayne Rashband, Research Services Branch, National Institutes of Health, Bethesda, MD). Each data set was collected in a single imaging session using identical filters, and exposure and illumination settings. Back-

ground images were obtained by imaging cell-free regions on each coverslip.

The image processing for Figure 2 began by subtracting the appropriate background image from each raw image to correct for uneven illumination. Image masks were then generated, correlating to the Golgi regions, as follows. It was not possible to select the Golgi regions by simple intensity thresholding of the images because thresholding values (i.e., pixel intensity ranges) to distinguish between adjacent bright fragments would not detect dimmer fragments (and vice versa). We circumvented this problem by subtracting from each image, a copy of itself that was blurred by convolving the image with a 5 × 5 mean neighborhood filter twice, and then the resultant image was segmented by eye (in comparison with the original image) and a binary "mask" that had values of "1" for the Golgi regions and "0" for all other regions of the image was created. These masks were then used for enumerating the Golgi fragmentation process with the cell boundaries defined by eye. The computer counted only fragments greater than 3 pixels in area; a pixel was measured to be approximately 0.219 μm in length. This image processing algorithm for distinguishing Golgi from non-Golgi regions was verified by comparing the computer-generated data with those of three separate and independent experimenters manually counting Golgi fragments from computer images and/or photographs.

The binary image masks were also used for application of a look-up table that roughly correlated with the concentration of the Golgi enzyme Galtf. Here the masks were multiplied with the background-subtracted images and the resultant images were then colored on a pixel by pixel basis as described in the caption of Figure 2. Intensity measurement errors due to out of focal plane fluorescence were most pronounced in the thicker portions of cells (in the perinuclear regions). Our interest, however, was how intensity values between sets of Golgi fragments in the cell periphery (in thinner cell regions) changed over time. To minimize errors in this analysis, we selected large flat cells to sample and used an objective with a deep depth of field (to image as many fragments per cell as possible). When serial Z-section slices (step size = 0.26 μm) of several cells were collected and inspected, we found that approximately 90% of the Golgi elements were detected by our approach. To verify that changes in fragment intensity at different times in nocodazole reflected changes in distribution of Galtf within the cell and not a loss or gain of total fluorescence signal, we compared total cellular fluorescence at these times. Using IPLab software a region of interest was drawn around each cell and the average fluorescence intensity per cell was measured for a minimum of 12 cells per time point after subtracting background fluorescence. The average intensity per cell in arbitrary fluorescence units (a.f.u.) fell within the ranges of 6×10^6 to 9×10^6 at all time points, with the average fluorescence at 1 h being $9 \times 10^6 \pm 10^6$ and at 10 h being $8.3 \times 10^6 \pm 10^6$ a.f.u. This indicates that the overall total fluorescence intensity changed very little during the course of the experiment.

Changes in area of Golgi fragments as a function of time in nocodazole were also examined using the binary image masks. Here, images were color coded based on their size (i.e., number of pixels per fragment). Our unpublished observations revealed that the area of peripheral fragments increased during the first 4 h of nocodazole treatment.

RESULTS

Fluorescence Imaging of Golgi Fragmentation Induced by Microtubule Disruption

To analyze Golgi dispersal during microtubule disruption we used digital fluorescence imaging techniques to follow the time course of this process. With such an approach we hoped to determine how quickly Golgi fragments are generated, the extent of fragmentation, and whether changes in concentration of Golgi enzymes within fragments occurs over time. Answers to these questions are crucial for evaluating different models of Golgi fragmentation and for providing a framework for investigating the responsible mechanisms.

Golgi dispersal was monitored in HeLa cells preincubated on ice (to depolymerize microtubules) and then warmed to 37°C in the presence of nocodazole. Under these conditions all microtubules detected with an anti-α tubulin antibody were depolymerized within 1 min of warmup (our unpublished observations). To follow the redistribution of Golgi membrane during nocodazole treatment, cells were fixed after progressive time intervals in the drug, permeabilized, and the Golgi enzyme marker Galtf was localized by indirect fluorescence microscopy. Digital images of representative cells were acquired using a fluorescence microscope system equipped with a cooled charge-coupled device. The number, size, relative fluorescence intensity, and distribution of Golgi fragments generated at different times after microtubule depolymerization were then analyzed. As described in MATERIAL AND METHODS, Golgi fragments were identified as punctate spots (from 4–40 pixels in size) that had fluorescence intensities above a minimal threshold that was easily distinguished by eye. Due to the flatness of these cells, greater than 90% of all Golgi fragments within cells could be observed in a single focal plane setting, with those fragments that were out of focus limited to the region above and below the nucleus.

As shown in Figure 1, Golgi fragments became apparent within 15 min of nocodazole treatment with 20–60 fragments detected per cell compared with one to four Golgi elements identified in untreated cells. The number of fragments per cell quickly rose during the first 90 min of nocodazole treatment to approximately 200 fragments per cell. Thereafter, the number of fragments leveled off, with the average number of fragments per cell remaining constant at approximately 250 for up to 14 h of nocodazole treatment. Similar shaped curves were seen in multiple experiments with HeLa, Chinese hamster ovary, and NRK cells using species-specific antibodies to Golgi resident proteins; however, the time course of the redistribution varied with cell type (our unpublished observations). When cycloheximide was added at the time of nocodazole treatment, no change in the rate or extent of Golgi fragmentation was observed, indicating that new protein synthesis was not required for the observed effects.

To follow the overall distribution and intensity of Golgi fragments generated with time of treatment in nocodazole, fluorescent intensity measurements from the Galtf-enriched Golgi fragments were collected. The distribution of Golgi fragments and fragment in-

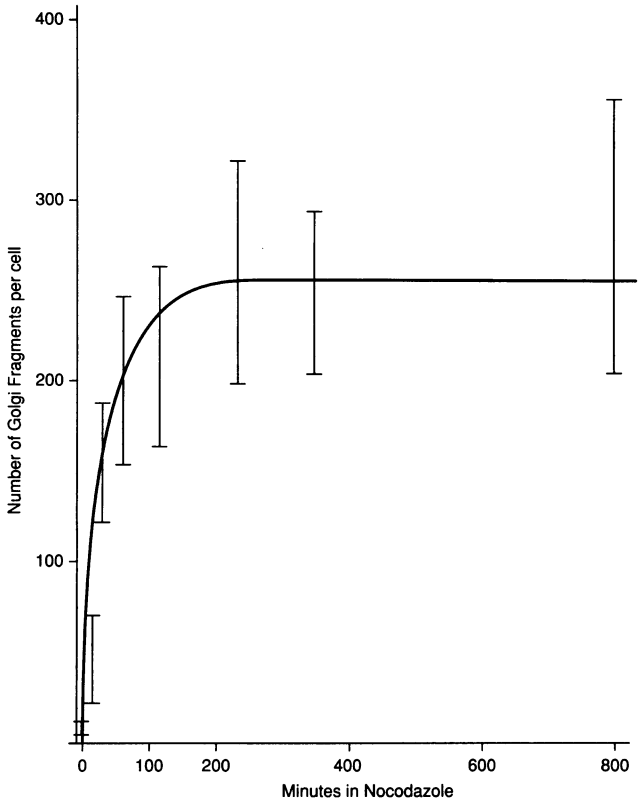

Figure 1. Time-dependent generation of Golgi fragments in nocodazole-treated cells. HeLa cells were incubated on ice for 10 min to depolymerize microtubules and then warmed to 37°C in the presence of nocodazole (1 μg/ml) for 0 s, 15 s, 30 s, 1 h, 2 h, 4 h, 6 h, and 14 h. Cells were then fixed, permeabilized, and stained with anti-Galtf antibodies followed by rhodamine-labeled goat anti-rabbit IgGs. The number of fragments per cell was then quantitated by counting spots (4–40 pixels in size) that had fluorescence intensities above a minimun threshold value that could be distinguished by eye (see MATERIALS AND METHODS). Fragment numbers per cell were then analyzed for 15 cells per time point and plotted as a function of time. The results show a rapid increase in fragment number, from between 1 and 5 at 0 min, to ~200 at 60 min. Thereafter, the number leveled off at approximately 250 fragments per cell for up to 14 h. Occasionally, some fragments were detected in a different focal plane. This was usually in the nuclear region and accounted for less than 10% of total fragments. The error bars represent the SD in fragment number per cell from analysis of 15 cells at each time point in the same experiment.

tensities within individual cells at different times of nocodazole treatment were then displayed after color coding Golgi fragments according to their intensity range, with the highest (2501–4095 a.f.u.) intensity fragments colored yellow, medium high (1001–2500 a.f.u.) intensity fragments blue, medium (501–1000 a.f.u.) intensity green, and lowest (20–500 a.f.u.) intensity red. At all times during the nocodazole treatment, the total cellular fluorescence (integrated) fell into the same range of values (see MATERIALS AND METHODS), indicating that changes in distribution of the Galtf-derived fluorescence reflected changes in distribution of this enzyme within the cell and not a loss or gain of total enzyme or fluorescence signal.

As shown in Figure 2, in untreated cells (0 min) Golgi elements were restricted to a single juxtanuclear location near the centrosome and had high (yellow) and medium high (blue) intensity values. At 15 min of nocodazole treatment, Golgi elements in central sites were still of very high intensity (yellow and blue), but a number of very low (red) intensity fragments began to appear throughout the cytoplasm. Although many of these fragments were in the vicinity of the central bright Golgi elements, some were surprisingly far removed from this centrosomal location. Between 30 and 60 min of nocodazole treatment, the number of peripheral Golgi fragments grew significantly until it leveled off at approximately 250 fragments per cell (see Figure 1). Strikingly, although the Golgi fragment number had leveled off by 90 to 120 min of nocodazole treatment, the intensity of individual fragments continued to change for up to 6 h. The originally bright central Golgi elements became dimmer with increasing times in nocodazole, while peripheral fragments became brighter. This indicated that Galtf continued to redistribute to peripheral fragments after the number of fragments had stopped increasing. After 6 h of nocodazole treatment, both peripheral and central Golgi fragments exhibited the same medium (green) intensity range. Addition of cycloheximide at the time of nocodazole treatment did not alter these results. Examination of the size of the peripheral fragments over time in nocodazole revealed that they increased in area during the first 4 h as well (see MATERIALS AND METHODS). These results are incompatible with a model of Golgi fragmentation based solely on fragmentation of Golgi stacks into increasingly smaller elements that disperse through the cytoplasm. Instead, they suggest a mechanism involving redistribution of Golgi enzymes to a limited number of peripheral sites that increase in size and in concentration of Golgi enzymes over time.

Differential Rates of Accumulation of ERGIC-53 and Galtf into Peripheral Fragments during Nocodazole Treatment

To test whether other Golgi membrane components redistributed at the same or different rates to peripheral sites, we compared nocodazole's effects on the distribution of Galtf with that of an itinerant Golgi marker, ERGIC-53 (Schweizer *et al.*, 1988, 1990). ERGIC-53 normally spends only a portion of its time in the Golgi complex as it rapidly cycles between the ER and Golgi complex (Hauri and Schweizer, 1992). It accumulates, however, in pre-Golgi and Golgi membranes upon lowering the temperature to 16°C for several hours (Lippincott-Schwartz *et al.*, 1990;

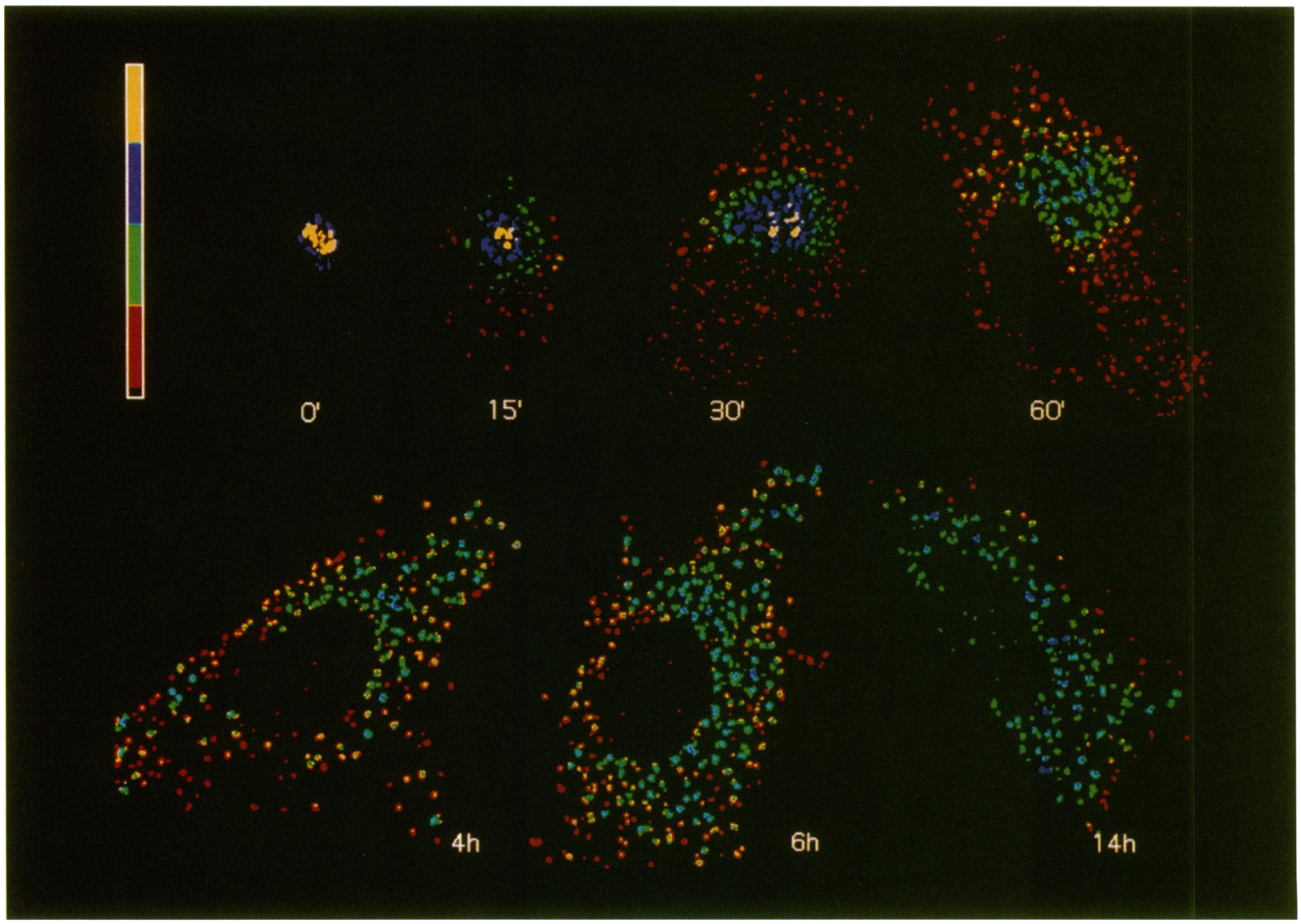

Figure 2. Changes in relative intensity and distribution of Golgi fragments over time in nocodazole-treated cells. Selected images of nocodazole-treated HeLa cells (stained with anti-Galtf antibodies and fluorescently labeled goat anti-rabbit IgGs) that were acquired from the experiment in Figure 1 were analyzed for relative fluorescence intensity and distribution of Golgi fragments (see MATERIALS AND METHODS). Representative individual cell images from 0, 15, 30, 60 min and 4, 6 and 14 h are shown. The intensity profiles of these cells is qualitatively represented by applying a five-color look-up table (see upper left corner) to these images. The colors represent a spectrum of 4096 gray levels (12 bits) with 0 being the dimmest, as follows: black (0–20 arbitrary fluorescence units, a.f.u.), red (21–500 a.f.u.), green (501–1000 a.f.u.), blue (1001–2500 a.f.u.), and yellow (2501–4095 a.f.u.). The intensity profile was selected simply to illustrate that the dispersal process was not a uniform spreading out and dimming of the original Golgi signal seen at the 0-min time point. Note that at earlier times numerous dim fragments were found in the cell periphery; however, with increasing times in nocodazole, the peripheral intensity levels increased significantly, suggesting a redistribution process had occurred.

Schweizer *et al.*, 1990) due to effects of reduced temperature on membrane traffic (Saraste and Kuismanen, 1984). Upon warmup to 37°C from 16°C, ERGIC-53 resumes cycling between the ER and Golgi, moving as a synchronous population into the ER before acquiring a steady-state distribution throughout the ER/Golgi system (Lippincott-Schwartz *et al.*, 1990). In the experiments described below we examined whether ERGIC-53 moves to the same or different sites as Galtf and how fast this redistribution occurs upon warmup from 16°C in the presence of nocodazole.

As shown in Figure 3, ERGIC-53 appeared colocalized with Galtf in a tight juxtanuclear structure representative of the Golgi complex after 3 h at 16°C. The ultrastructural distribution of ERGIC-53 at this temperature is shown in Figure 4. Peroxidase reaction product was localized within Golgi cisternae, as well as within surrounding vesicles, indicating that ERGIC-53 had distributed within Golgi membranes at this temperature. Strikingly, within 5 min of warmup to 37°C from 16°C (see Figure 3), ERGIC-53 had moved out of the central Golgi region and was localized throughout the ER, including the nuclear envelope. After 10 min at 37°C, the pattern of ERGIC-53 staining was no longer restricted to the ER but became concentrated in numerous discrete

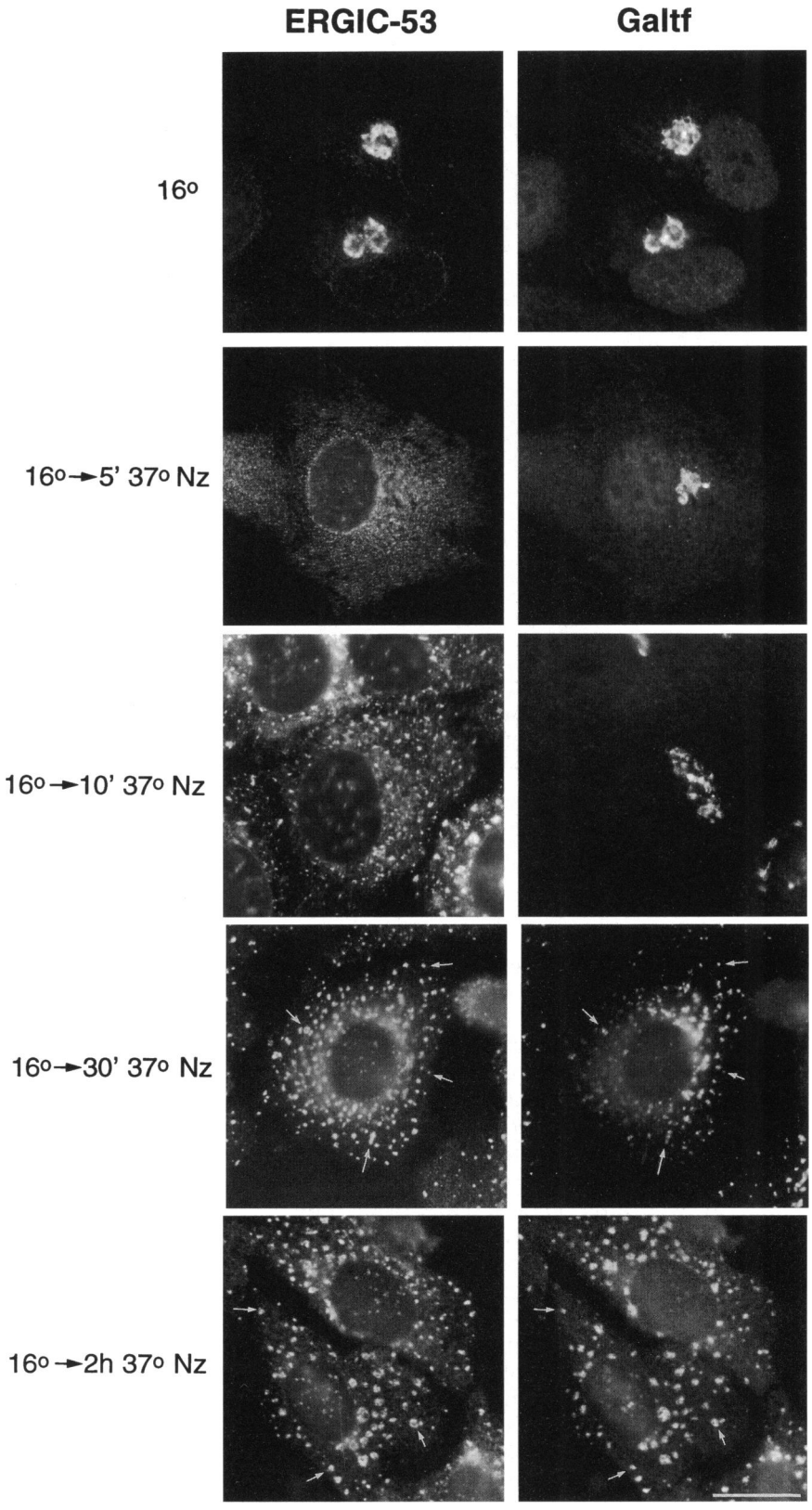

Figure 3. Golgi-localized ERGIC-53 and Galtf redistribute at distinct rates to peripheral fragments during nocodazole treatment. M1 human fibroblasts were incubated for 3 h at 16°C. The cells were then placed on ice for 10 min to depolymerize microtubules and warmed to 37°C for the indicated times in the presence of nocodazole (1 μg/ml). Cells were fixed, permeabilized, and stained with mouse anti-ERGIC-53 antibody and rabbit anti-Galtf antibody, followed by rhodamine-conjugated goat anti-mouse IgGs and fluorescein-conjugated goat anti-rabbit IgGs. Arrows point to peripheral structures where ERGIC-53 and Galtf are co-distributed. This occurred within 30 min of nocodazole treatment at 37°C. Note that only a small subset of the ERGIC-53–containing fragments at this time contained Galtf, and peripheral fragments containing Galtf always contained ERGIC-53. After 2 h of nocodazole treatment, the majority of ERGIC-53–containing fragments contained Galtf. Bar, 10 μm.

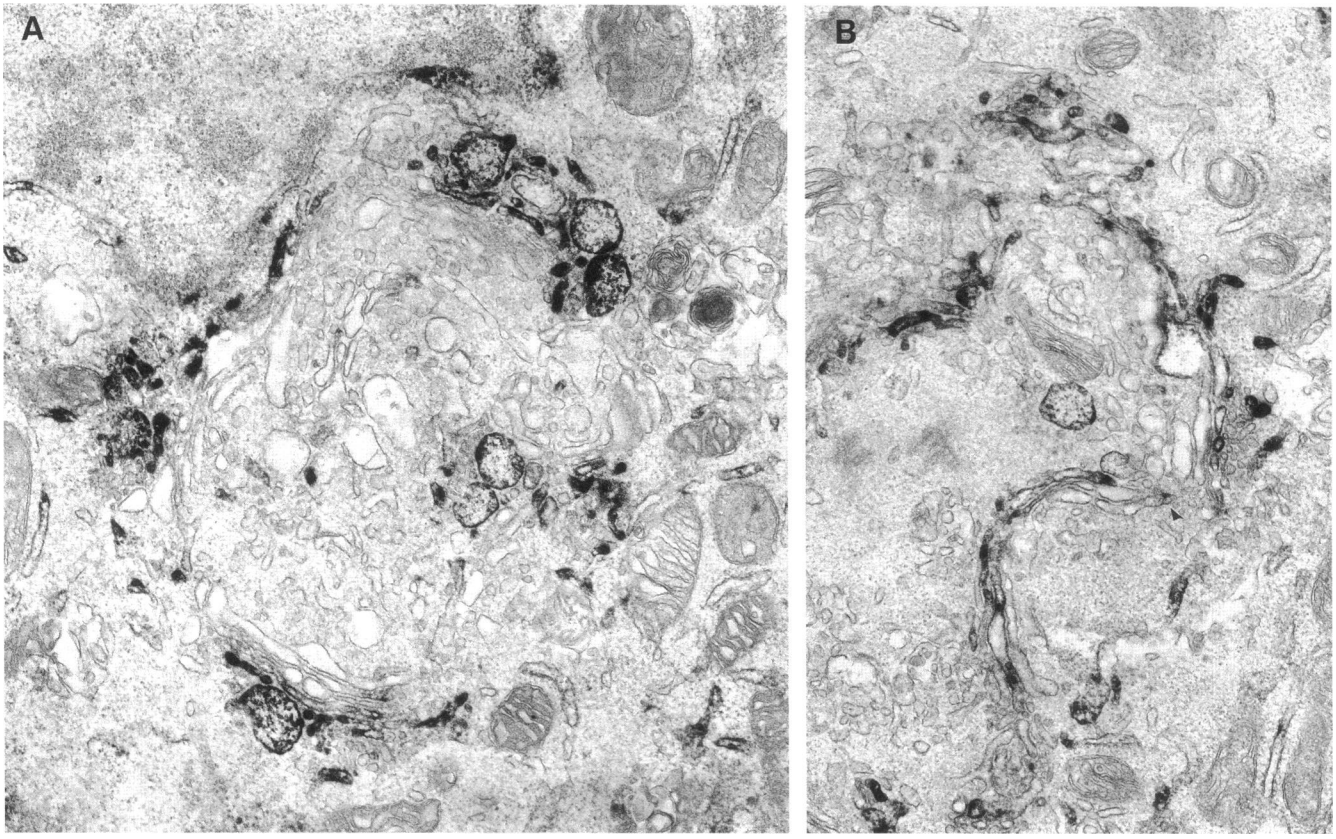

Figure 4. Redistribution of ERGIC-53 into Golgi cisternae in cells incubated at 16°C. M1 human fibroblasts were incubated at 16°C for 3 h. The cells were then fixed, permeabilized with saponin, and labeled with anti-ERGIC-53 antibodies followed by HRP-conjugated goat anti-mouse IgG. After reaction with diaminobenzidine hydrochloride, H_2O_2, the cells were prepared for electron microscopy. HRP reaction product was found associated primarily with Golgi stacks and nearby vesicular intermediates. (A and B) Golgi regions from two different cells. Note that ERGIC-53 labeling appeared to be most enriched in the *cis*-most Golgi cisternae of Golgi stacks.

structures distributed throughout the cell. Accumulation of ERGIC-53 in these structures was more pronounced after 30 min at 37°C and remained associated with these peripheral structures for more than 2 h of nocodazole treatment.

The distribution of Galtf was restricted to central Golgi elements at the earliest time at 37°C in nocodazole-treated cells, when ERGIC-53 had already accumulated in peripheral structures (see Figure 3, 10 min). However, after 30 min, many of the ERGIC-53–containing fragments also contained small quantities of GalTf (Figure 3, see arrows). By 2 h at 37°C in nocodazole, this co-localization was dramatic, with virtually every ERGIC-53–containing fragment also containing significant quantities of Galtf. Significantly, at no time during nocodazole treatment was Galtf ever observed in fragments that did not also contain ERGIC-53. Identical results were obtained in experiments where cycloheximide was included in the incubation medium. These results indicate, therefore, that itinerant (i.e., ERGIC-53) and resident (i.e., Galtf) Golgi markers redistribute at distinct rates from central Golgi structures to the same peripheral sites upon nocodazole treatment, with ERGIC-53 redistributing rapidly to these sites after first cycling through the ER, and Galtf redistributing more slowly. Additional experiments in cells whose temperature was never lowered to 16°C showed that upon nocodazole treatment, ERGIC-53 also quickly changed its distribution from a diffuse distribution including the ER and Golgi complex (see Lippincott-Schwartz *et al.*, 1990) to discrete peripheral sites where Galtf later redistributed (our unpublished observations). Thus, whether ERGIC-53 is localized to the Golgi (i.e., at 16°C) or throughout the ER/Golgi system (at 37°C) did not affect its final distribution at 37°C in nocodazole.

Peripheral Golgi Elements Generated during Microtubule Disruption Reside Adjacent to Sites of Membrane Export from the ER

The observation that Galtf-containing peripheral Golgi elements generated during nocodazole treatment localize to sites of accumulation of ERGIC-53 led

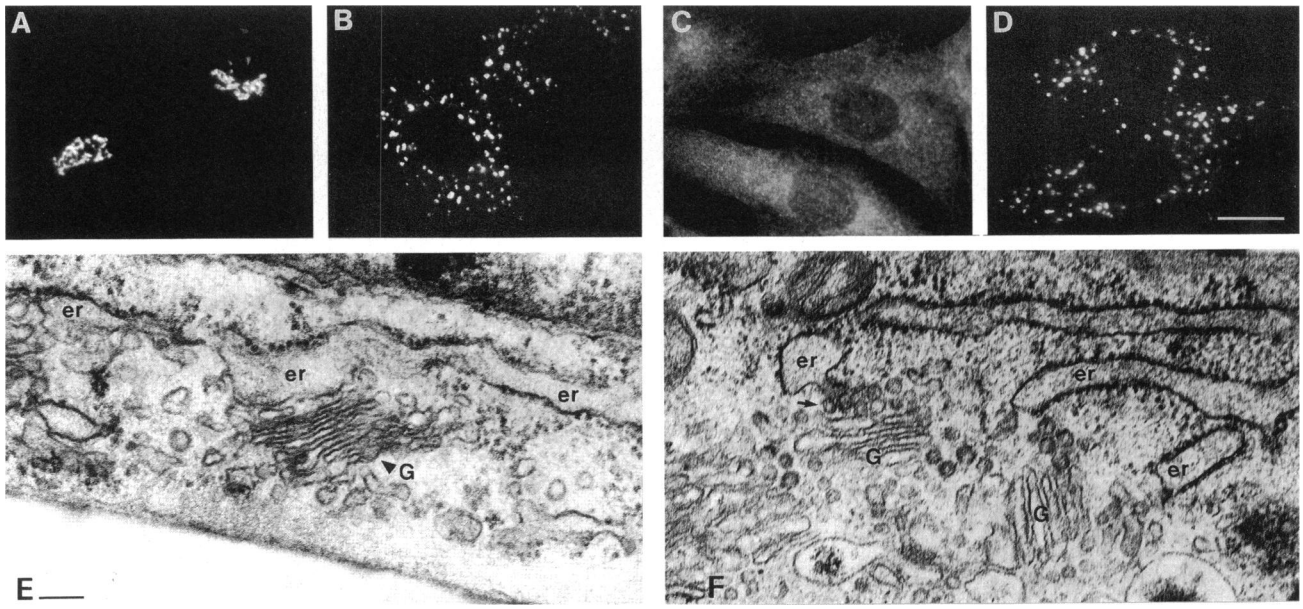

Figure 5. Golgi fragments adjacent to ER membranes are formed during nocodazole treatment whether Golgi membrane originates from cisternal stacks in the cell center or from the ER. (A, B, and E) NRK cells were treated with nocodazole (B and E) or without (A) at 37°C for 2 h and then fixed and permeabilized. Samples were either stained for immunofluorescence microscopy using Man II antibodies followed by rhodamine-labeled goat anti-mouse IgGs (A and B) or processed for electron microscopy (E). (C, D, and F) NRK cells were treated with BFA for 30 min at 37°C (C), placed on ice for 10 min, and then washed free of the drug for 30 min in the presence of nocodazole (D and F). After fixation and permeabilization, samples were either prepared for immunofluorescence using Man II antibodies (C and D) or processed for electron microscopy (F). er, endoplasmic reticulum; and G, Golgi complex. The arrowhead in panel E points to Golgi stacks, while the arrow in F points to vesicles budding from ER that are adjacent to Golgi stacks. Bar in panel D, 10 μm; bar in panel E, 0.15 μm.

us to investigate further the morphology and localization of these structures. As shown by electron microscopy in Figure 5E, Golgi elements appeared as discrete mini-stacks after 2 h of nocodazole treatment and were intimately associated with regions of the ER where budding of membrane was apparent. For every set of Golgi stacks observed, budding ER membrane profiles could be seen at nearby sites. The close spatial association of peripheral, mini-Golgi stacks with the ER was even more striking at the light microscopic level. As shown in Figure 6 (A and B), immunofluorescence double labeling with the *cis*/medial Golgi marker Man II and an ER marker in cells treated with nocodazole for 4 h showed Man II to be distributed at discrete sites adjacent to the elaborate network of ER membranes with virtually no staining in regions of the cytoplasm devoid of ER. In several places, co-distribution of red fluorescence from Man II staining and green fluorescence from ER labeling was significant enough to produce a yellow signal, indicative of an overlap in the distribution of the two markers. In contrast to Golgi markers, fluorescence staining of endosomal and lysosomal markers in nocodazole-treated cells revealed these markers to fill the spaces devoid of the ER (our unpublished observations).

To further characterize the localization of Golgi fragments generated during nocodazole treatment, we compared the distribution of Golgi fragments with that of the temperature-sensitive viral glycoprotein, ts045 VSV G (VSV G) (Bergmann, 1989) upon release of this glycoprotein from the ER under conditions where transport is slowed (at 16°C or 20°C) (Griffiths *et al.*, 1989; Saraste and Kuismanen, 1992) or limited (for 10 min at 32°C). VSV G protein is unable to fold properly and generally cannot exit the ER in cells infected with the ts045 strain of the vesicular stomatis virus that are incubated at 40°C (DeSilva *et al.*, 1990). Upon lowering the temperature to 32°C, however, proper folding occurs and VSV G rapidly exits the ER moving into the Golgi complex enroute to the cell surface. Infected cells were incubated for several hours in nocodazole at 40°C to accumulate VSV G in the ER while allowing Golgi enzymes to redistribute into peripheral fragments. The temperature was then lowered to 32°C for 10 min, or to 16°C or 20°C for 30 min in the continued presence of nocodazole to allow export of VSV G from the ER. Each of these conditions (see Figure 7 for 32°C for 10 min and 20°C for 30 min) resulted in the complete co-localization of VSV G in Man II-containing structures. Before Golgi fragmentation, however, a significant proportion of VSV G

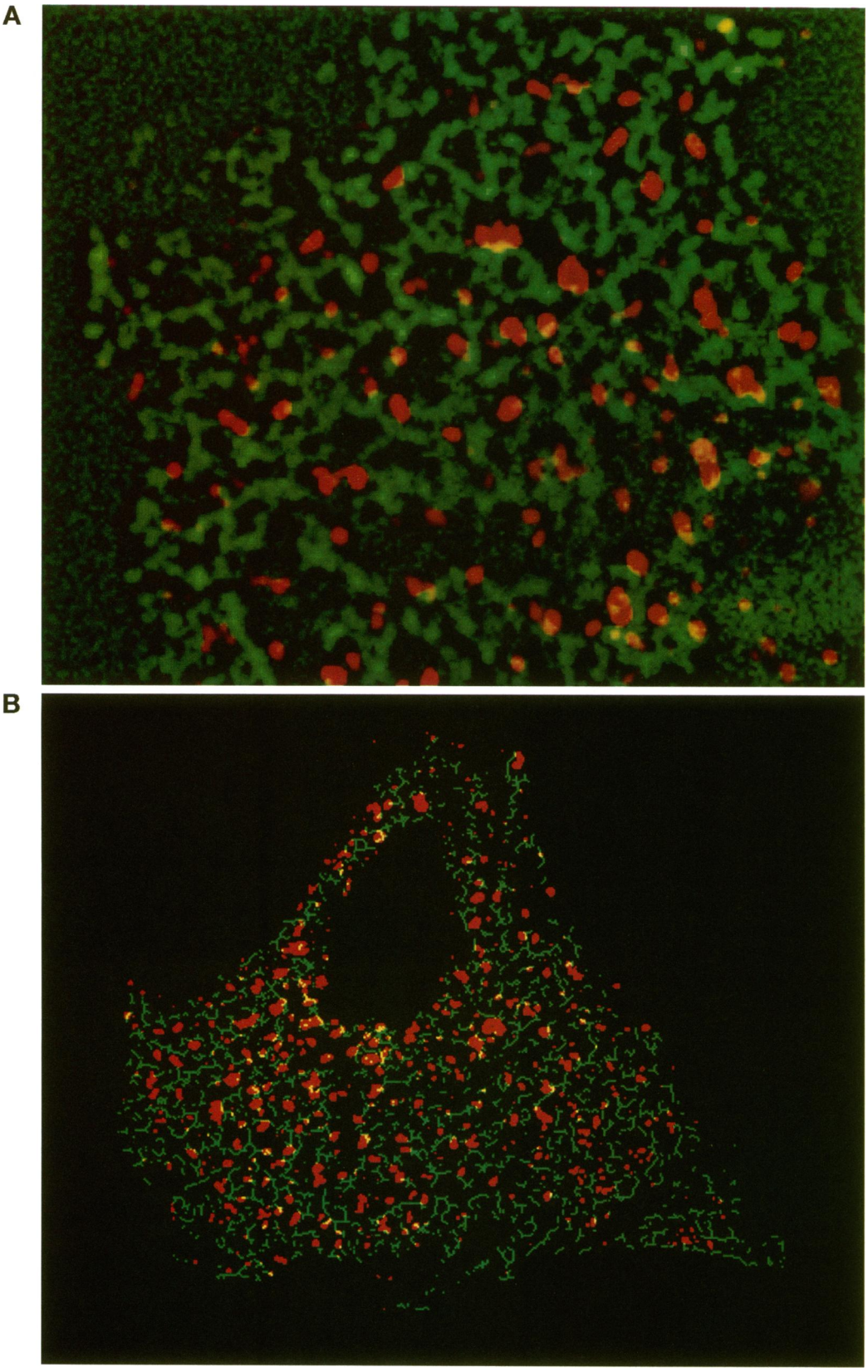

Figure 6. Distribution of Golgi and ER markers after long term nocodazole treatment. (A) NRK cells were incubated with nocodazole for 4 h at 37°C, fixed, permeabilized, and labeled with mouse monoclonal antibody to Man II and a rabbit antibody to ER membranes followed by fluorescein-labeled goat anti-rabbit IgGs and rhodamine-labeled goat anti-mouse IgGs. Separate Golgi (red) and ER (green) images were collected and processed. The image processing procedure consisted of a subtraction of a pseudo-background image for the purpose of revealing staining character, and then adding color and overlaying the image pair and enlarging a region roughly 8–10 μm in length. Note the spatial alignment of Golgi fragments nestled within regions of the ER. Yellow regions indicate overlap in staining with the two fluorophores. (B) Lower magnification image of the cell shown in panel A. The image processing procedure consisted of overlaying the Golgi image onto the ER image that had been processed using IP Lab Spectrum's skeletonization algorithm to reveal the reticular pattern of the ER. Weakly stained ER strands were lost during this process. Note that Golgi fragments invariably were found in close association with ER membranes.

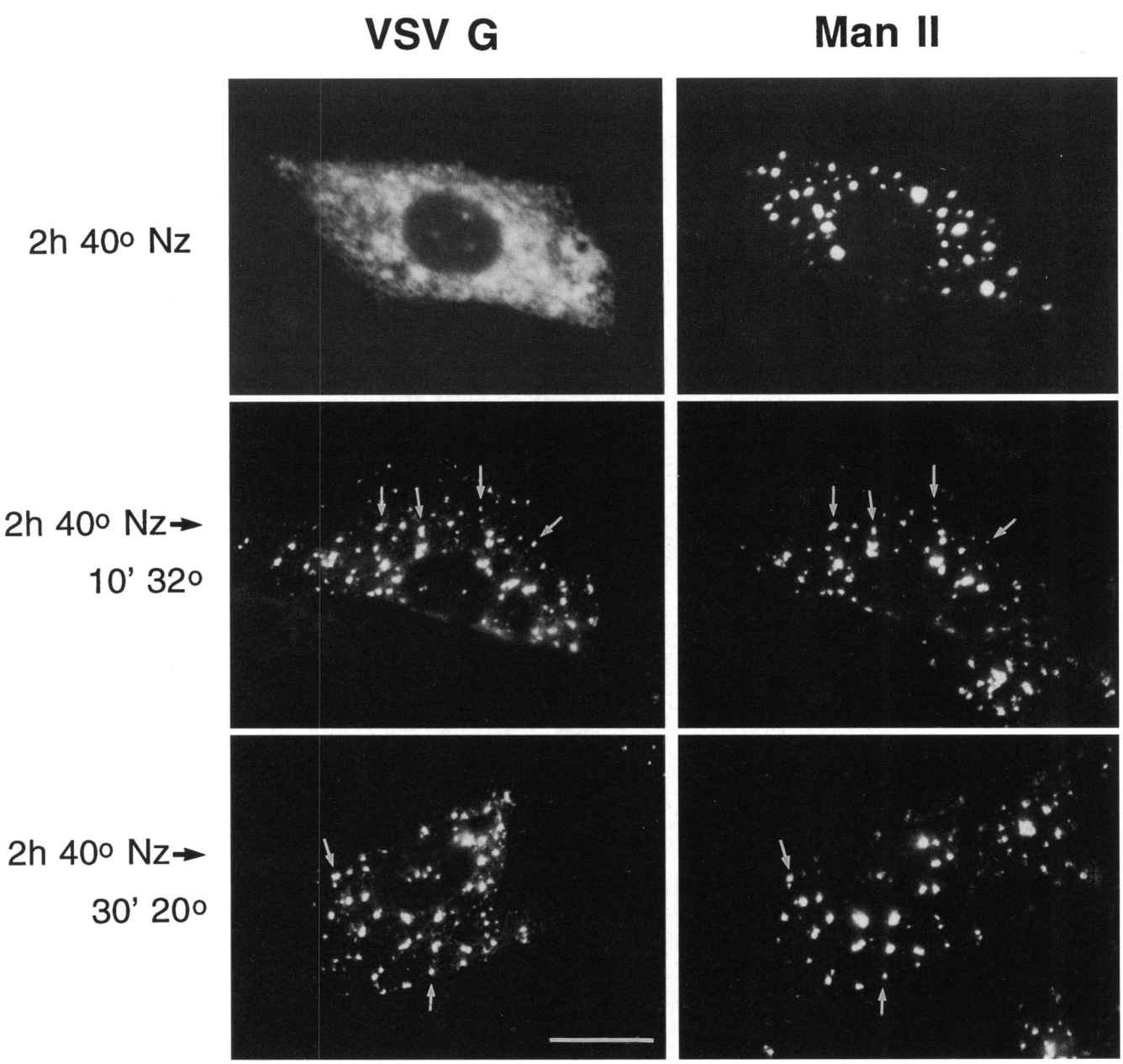

Figure 7. Nocodazole-induced Golgi fragments reside at peripheral sites where VSV G is released from the ER. NRK cells infected with ts045 VSV were incubated at 40°C for 4 h with nocodazole added during the last 2 h of incubation to cause the Golgi to fragment to peripheral sites. Cells were then fixed (top panels), or incubated at 32°C for 10 min in nocodazole (middle panels), or at 20°C for 30 min in nocodazole (bottom panels) before fixation. After permeabilization, cells were incubated with mouse anti-VSV G antibody and rabbit anti-Man II antibody, followed by rhodamine-conjugated goat anti-mouse IgGs and fluorescein-conjugated goat anti-rabbit IgGs. The results show that upon release from the ER at 32°C for 10 min or at 20°C for 30 min, VSV G co-distributes with Man II-containing fragments (see arrows). Bar, 10 μm.

newly released from the ER in nocodazole-treated cells did not co-localize with Man II (see below). These results suggest, therefore, that Man II-enriched Golgi fragments generated during nocodazole are localized in close proximity to sites where VSV G is released from the ER.

Effects of Microtubule Disruption on Anterograde, ER-to-Golgi Traffic

VSV G released from peripheral ER sites remained localized to peripheral sites during incubations at 32°C in the presence of nocodazole, and never clustered into the centrosomal region (see Figure 8, third

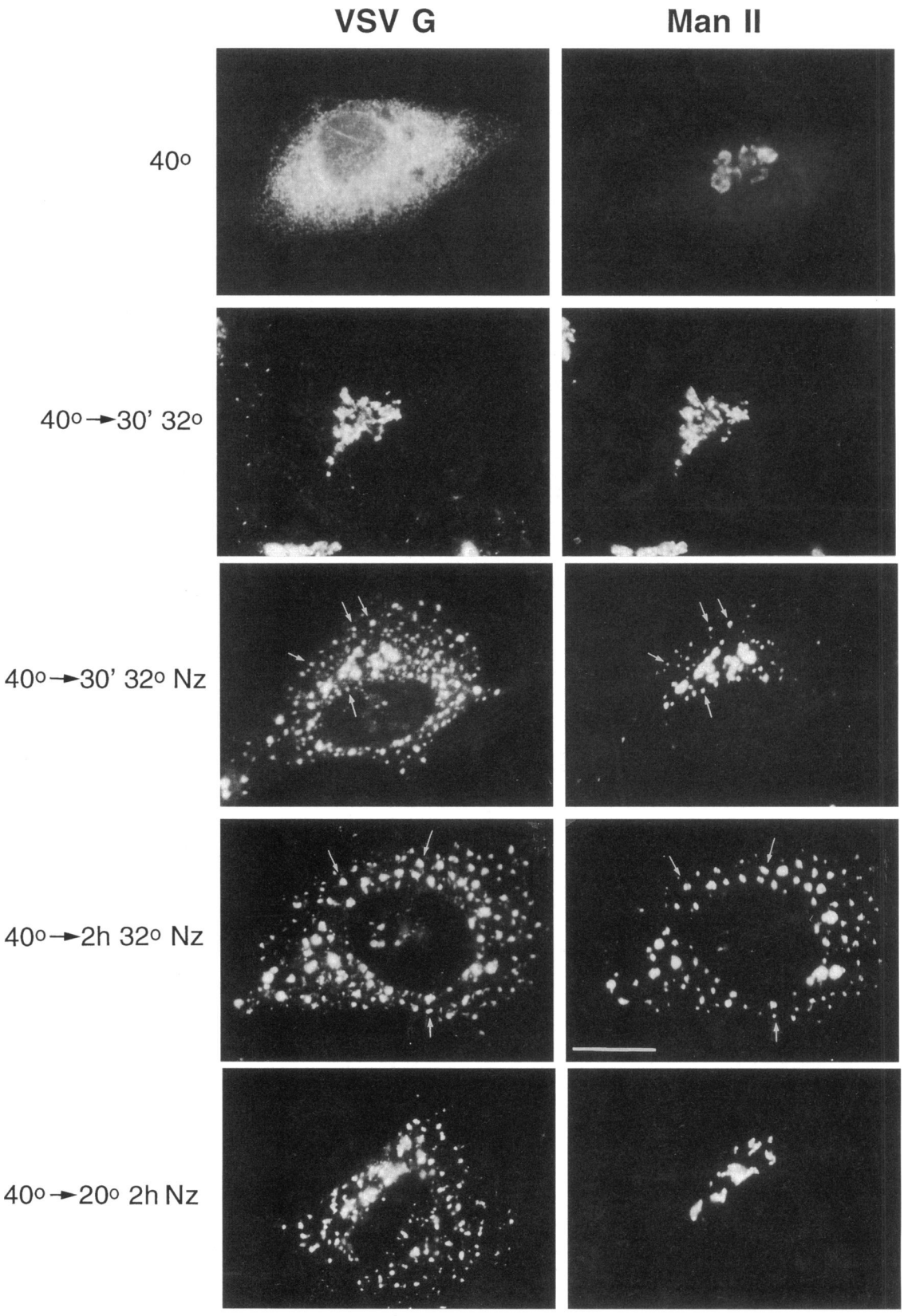

Figure 8.

and fourth panels down). This was in contrast to untreated cells where VSV G completely redistributed into the central Golgi region after 30 min of shifting the temperature from 40°C to 32°C (Figure 8, second panel down). The peripheral structures containing VSV G in nocodazole-treated cells were labeled with antibodies to the coatomer subunit, βCOP (Lippincott-Schwartz *et al.*, 1995), suggesting that they functioned as ER-to-Golgi trafficking intermediates (Pepperkok *et al.*, 1993; Peter *et al.*, 1993; Griffiths *et al.*, 1995), and upon removal of nocodazole redistributed into the centrosomal region (our unpublished observations). These results indicate that microtubules are necessary for the translocation into the centrosomal region of peripheral transport intermediates carrying VSV G newly released from the ER.

After long periods (i.e., 30 min or more) of nocodazole treatment Man II began to appear in peripheral VSV G-containing structures (Figure 8, see arrows) and by 2 h was completely localized with VSV G in peripheral structures. This process was analogous to the nocodazole-induced redistribution of Galtf to ER-GIC-53-containing peripheral structures illustrated in Figure 3. Significantly, redistribution of Man II to peripheral structures containing VSV G was sensitive to temperature and did not occur in cells incubated at 20°C in nocodazole. This observation is consistent with data from Turner and Tartakoff (1989) demonstrating failure of Golgi membranes to disperse at reduced temperatures in nocodazole-treated cells.

The above results suggest that the effect of microtubule depolymerization on anterograde, ER-to-Golgi traffic varies depending on the localization of the Golgi complex. After early times of nocodazole treatment (when the Golgi is still centrosomally localized), transport of membrane from peripheral ER exit sites to the Golgi is inhibited (see Figure 8, third panel). After prolonged exposure of cells to nocodazole, however, when Golgi enzymes redistribute to ER exit sites, transport is no longer blocked (see Figure 7, second panel). This interpretation predicts that Golgi processing of newly synthesized glycoproteins should be significantly inhibited after short periods of nocodazole treatment, because peripheral pre-Golgi intermediates that transport these proteins are incapable of clustering into the centrosomal region where Golgi enzymes are concentrated. After longer periods of nocodazole treatment, however, due to redistribution of Golgi enzymes to peripheral, pre-Golgi sites, processing of these glycoproteins should occur.

To test this hypothesis, we examined the rate at which metabolically pulse-labeled VSV G proteins are converted to endo H resistance upon release from the ER in cells treated with or without nocodazole. As shown in Figure 9, newly synthesized VSV G molecules in untreated cells were completely processed to endo H resistance within 20 to 30 min of chase at 32°C after pulse labeling. By contrast, in cells treated with nocodazole at the time of chase, the rate of processing of VSV G molecules to endo H resistance was significantly delayed and was not complete until approximately 90–120 min. This delay in processing of VSV G in nocodazole appeared to correlate to the rate of redistribution of Golgi membrane to peripheral sites (i.e., fragmentation), which occurs over 90–120 min in these cells. Consistent with this possibility, in cells pretreated in nocodazole for several hours (resulting in Golgi fragmentation) before pulse labeling, the rate of acquisition of endo H resistance of VSV G upon chase was as rapid as in untreated cells. However, in cells treated with nocodazole for 2 h at 20°C (which prevents Golgi fragmentation; see Figure 8, bottom panel), subsequent labeling and chase at 32°C in the continued presence of nocodazole resulted in a delayed rate of processing similar to cells treated with nocodazole at 32°C at the start of the chase. These results indicate that Golgi enzyme processing of newly synthesized VSV G is inhibited at early times after microtubule depolymerization and that Golgi fragmentation appears to be necessary for the complete processing of VSV G observed at later times.

Figure 8 (cont). Effect of nocodazole and reduced temperature on anterograde transport of VSV G into the Golgi complex. NRK cells infected with ts045 VSV were incubated at 40°C for 2h to accumulate VSV G in the ER. The cells were then fixed (top panel, 40°C) or placed on ice for 10 min and warmed to 32°C for 30 min in the absence of nocodazole (second panel down), to 32°C for 30 min in nocodazole (third panel down), to 32°C for 2 h in nocodazole (fourth panel down), or to 20°C for 2 h in nocodazole (bottom panel) before fixation. Cells were then permeabilized and incubated with mouse anti-VSV G antibody and rabbit anti-Man II antibody, followed by rhodamine-conjugated goat anti-mouse IgGs and fluorescein-conjugated goat anti-rabbit IgGs. Examination of the samples by fluorescence microscopy revealed that incubation in medium containing nocodazole impeded transport of peripherally distributed VSV containing structures into the centrosomal region. Upon longer treatments with nocodazole at 32°C, Man II redistributed from this centrosomal region to peripheral sites containing VSV G. Incubation with nocodazole at 20°C, however, blocked Golgi redistribution to peripheral sites. Very faint staining of VSV G could be observed on the cell surface after 2 h of chase in nocodazole at 32°C, indicating Golgi-to-surface transport occurred under these conditions. Bar, 10 μm.

Relationship between Golgi Fragmentation and Retrograde, Golgi-to-ER Traffic

Active membrane transport has previously been implicated in the Golgi dispersal process induced by microtubule disruption (Turner and Tartakoff, 1989). Consistent with this, we found that both Galtf and ERGIC-53 failed to redistribute to peripheral structures during nocodazole treatment and remained in central Golgi structures when the cells were exposed to the membrane traffic perturbants NEM, AlF, DOG/azide, or monensin (see Table 1), in contrast to treat-

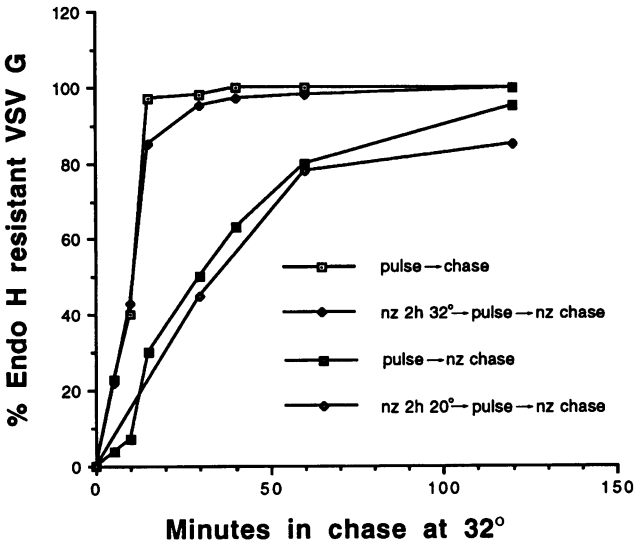

Figure 9. Differential effects of nocodazole on Golgi processing of VSV G and its relationship to Golgi fragmentation. NRK cells infected with ts045 VSV were placed on ice for 10 min, metabolically pulse-labeled with [^{35}S]methionine for 5 min at 32°C and then chased at 32°C under the following conditions: with no nocodazole added (pulse → chase); with nocodazole added at the time of chase (pulse → nz chase); with nocodazole added for 2 h at 32°C before pulse labeling and during the chase (nz 2 h 32°C → pulse → nz chase); or with nocodazole added for 2 h at 20°C before pulse labeling and during the chase at 32°C (nocodazole pretreated at 20°C). At the indicated time points, cells were solubilized in detergent and VSV G protein immunoprecipitated from cell lysates. Immunoprecipitates at each chase point were digested with endo H and separated by SDS-PAGE. The percentage of endo H-resistant VSV G was quantitated from autoradiograms scanned using a Molecular Dynamics scanning system. The results show a significant delay in processing of VSV G to endo H resistance under conditions where Golgi membrane reside in juxtanuclear sites at the start of the chase (i.e., in cells treated with nocodazole at the time of chase and in cells pretreated with nocodazole at 20°C, see Figure 8). In contrast, under conditions where Golgi membrane is fragmented at the start of the chase (i.e., pretreatment with nocodazole at 32°C), rapid acquisition of endo H resistance by VSV G was observed. This suggests that Golgi fragmentation after microtubule disruption is required for efficient processing of newly synthesized proteins by Golgi enzymes.

ment with cytochalasin D (which disassembles the actin cytoskeleton), which had no effect on the Golgi dispersal process.

The observation that different molecules associated with the Golgi complex (i.e. Galtf and ERGIC-53 in human fibroblasts) redistribute at distinct rates to peripheral fragments during nocodazole treatment, and that ERGIC-53 follows a Golgi-to-ER retrograde transport pathway enroute to peripheral Golgi fragment sites during nocodazole treatment (see Figure 3), led us to investigate whether retrograde transport played any role in Golgi dispersal. The effect of microtubule disruption on retrograde traffic of ERGIC-53, observed upon warming of cells from 16°C, and on Man II after treatment with BFA, a drug which induces exaggerated retrograde transport of Golgi proteins (Lippincott-Schwartz *et al.*, 1990; Klausner *et al.*, 1992), was examined. Cells were incubated on ice for 10 min and were then warmed to 37°C (for ERGIC-53) or treatment with BFA at 37°C in the presence or absence of nocodazole (for Man II). The extent of redistribution of these molecules out of Golgi structures and into the ER was then assessed using immunofluorescence microscopy. As shown in Figure 10, A and B, nocodazole treatment slowed, but did not block retrograde transport of both ERGIC-53 and Man II, in contrast to NEM, monensin, or DOG/azide treatments, which each significantly inhibited retrograde transport. For ERGIC-53, microtubule depolymerization increased the half-time for transport into the ER by only a few minutes, while for Man II, microtubule disruption increased the half-time of retrograde transport slightly more, from 3–5 min to 15–20 min. These combined results (Figure 10 and Table 1) indicate that microtubules facilitate but are not required for retrograde transport and that drugs that block retrograde traffic also prevent Golgi dispersal during microtubule disruption.

To further investigate the relationship between retrograde traffic and Golgi dispersal, we treated cells with BFA to redistribute Golgi enzymes into the ER and then removed BFA in the presence of nocodazole. As shown in Figure 5 (D and F), the fate of Golgi enzymes under these conditions was indistinguish-

Table 1. Inhibitors of nocodazole-induced redistribution of ERGIC-53 and Galtf to peripheral sites

Inhibitor	% Cells with ERGIC-53 in peripheral structures after nocodazole-treatment	% Cells with Galtf in peripheral structures after nocodazole-treatment
—	100%	100%
NEM	2%	3%
AlF	21%	16%
DOG/azide	20%	22%
Monensin	12%	18%
20°	15%	12%
Cytochalasin D	100%	100%

Human M1 fibroblasts were incubated for 3 h at 16°C, placed on ice for 10 min, and warmed to 37°C or 20°C in the presence of nocodazole with the indicated drugs added. After 30 min (for assessing effects on ERGIC-53) and 90 min (for assessing effects of Galtf) cells were fixed, and the distribution of ERGIC-53 and Galtf was examined by immunofluorescence double labeling. For determining the percentage of cells with ERGIC-53 redistributed to peripheral fragments after nocodazole treatment, cells with ERGIC-53 completely redistributed to peripheral sites were scored positive for redistribution. For determining the percentage of cells with Galtf redistributed into peripheral fragments during nocodazole treatment, cells showing any evidence of Galtf in peripheral fragments were scored positive for redistribution. Between 150–200 cells were counted per condition.

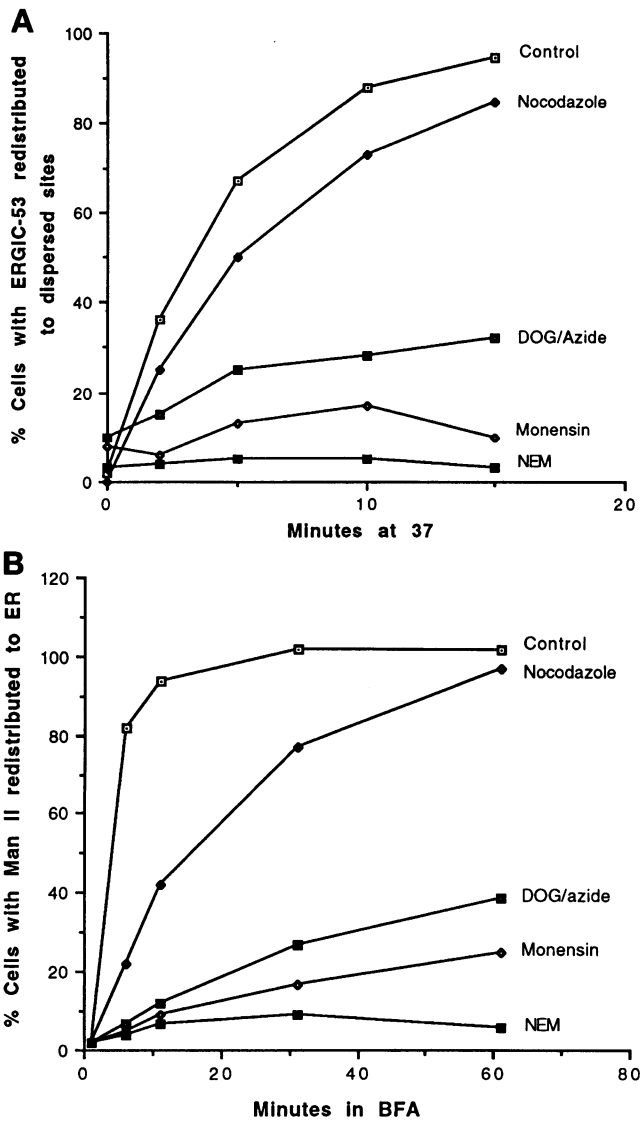

Figure 10. Inhibitors of Golgi-to-ER retrograde transport of ERICG53 and Galtf. (A) To assess the effects of different reagents on retrograde transport of ERGIC-53, M1 fibroblasts were first incubated for 3 h at 16°C to accumulate ERGIC-53 in central Golgi structures. Ten minutes before warmup, cells were treated with NEM (0.5 mM), monensin (10 uM), DOG (50 mM)/azide (.02%), nocodazole (5 uM), or nothing. Cells were then warmed to 37°C in the continued presence of the drugs. At the indicated times cells were fixed, permeabilized, and stained with mouse anti-ERGIC-53 antibody and rabbit anti-Galtf antibody followed by rhodamine-conjugated goat anti-mouse IgGs and fluorescein-conjugated goat anti-rabbit IgGs. To determine the percentage of cells with ERGIC-53 in dispersed sites, only those cells with ERGIC-53 completely dispersed (showing no co-localization with Galtf in central Golgi structures) were scored positive and the results plotted in graph form. Between 150–200 cells were examined per time point. (B) The effects of different reagents on BFA-induced retrograde transport of Man II into the ER were measured in NRK cells. Ten minutes before BFA treatment, cells were incubated with nocodazole (nz), DOG/azide, monensin, NEM, or nothing. Cells were then treated with BFA (1 μg/ml) at 37°C in the continued presence of the drugs. At the indicated times, cells were fixed, permeabilized, and

able from cells treated with nocodazole alone. After 30 min of BFA washout in nocodazole-treated cells, Man II became localized to numerous peripheral structures scattered throughout the cytoplasm (see Figure 5, D and F). Not only was the average number of Golgi fragments per cell under these conditions no different than in cells treated with nocodazole alone (our unpublished results), but the ultrastructure of individual fragments resembled cells treated with nocodazole alone (compare Figure 5, E and F). These fragments consisted of stacks of short cisternae localized next to membrane budding sites of the ER (Figure 5F, see arrow), and were functionally competent for protein secretion as determined from metabolic pulse chase experiments (our unpublished observations). These results indicate that functional Golgi stacks scattered in the cell periphery can be rapidly assembled de novo from Golgi membrane components that have followed a retrograde pathway into the ER and then been exported out again in the presence of nocodazole. The Golgi stacks remained localized to ER exit sites as long as microtubules were depolymerized, and reclustered into the centrosomal region upon microtubule repolymerization (our unpublished observations).

DISCUSSION

It has been known for years that microtubule disruption with agents like nocodazole have dramatic effects on Golgi morphology, with hundreds of functional Golgi units now appearing throughout the cytoplasm (Pavelka and Ellinger, 1983; Rogalski and Singer, 1984; Thyberg and Moskalewski, 1985; Turner and Tartakoff, 1989). How this profound redistribution of Golgi membrane occurs without disrupting secretory flow from the ER is unknown. The most common thinking is that Golgi fragments generated during microtubule depolymerization arise from random diffusion within the cytoplasm of Golgi ministacks no longer tethered to microtubules. In this paper, we have drawn upon a wide variety of techniques and approaches to evaluate different models of Golgi fragmentation during nocodazole treatment and demonstrate convincingly that this is not the case. Our results reveal that after microtubule disruption the Golgi complex rebuilds itself into hundreds of ministacks in the cell periph-

(Figure 10 cont.) labeled with mouse anti-Man II followed by rhodamine-conjugated goat anti-mouse IgGs. For determining the percentage of cells with Man II in the ER, only those cells with Man II completely redistributed into the periphery were scored positive. Cells (150–200) were examined per time point and the data presented in graph form.

ery adjacent to ER exit sites. Before this redistribution, secretory flow from the ER to the Golgi is profoundly disrupted and only returns to normal levels after Golgi enzymes redistribute to peripheral ER exit sites where Golgi stacks are regenerated. As discussed below, these results shed new light on potential mechanisms of Golgi fragmentation, on roles of microtubules in membrane traffic between the ER and Golgi, and on the extent of retrograde traffic by Golgi enzymes.

Potential Mechanisms of Golgi Fragmentation

The first indication that fragmentation of the Golgi complex during nocodazole treatment was not due to simple diffusion of Golgi elements through the cytoplasm came from quantitative fluorescence imaging studies examining the rate and extent of fragmentation over time, and temporal changes in the distribution of Golgi membrane components within fragments. The data revealed that fragmentation proceeded by a process where a limited number of fragments (approximately 250 per cell) were generated relatively early after nocodazole treatment and remain constant for up to 14 h thereafter. Although the ER/Golgi cycling molecule, ERGIC-53, redistributed to the fragment sites within 10 min of nocodazole treatment, Man II and Galtf redistributed gradually over several hours. Both the relative concentration of Golgi enzymes within these fragments (as assessed by quantitative fluorescence imaging of Galtf in the absence of new protein synthesis) and the fragment size increased over time during nocodazole treatment, consistent with fragment growth.

Remarkably, Golgi fragments generated during nocodazole treatment were found to reside adjacent to ER exit sites. Multiple approaches were taken to support this conclusion, including electron microscopy, fluorescence co-localization of Golgi markers with ER markers, co-localization of Golgi markers with VSV G released from the ER at 16°C and 20°C, and co-localization of Golgi markers with ERGIC-53. Ultrastructural examination of the fragments revealed many to consist of mini-stacks. That Golgi-derived components were capable of building these stacks de novo upon export out of the ER was supported in experiments where ER-retained Golgi enzymes in BFA-treated cells were released from the ER during BFA washout in the presence of nocodazole. The number, distribution, and morphology of peripheral Golgi structures formed after this treatment were indistinguishable from that of Golgi structures generated during nocodazole treatment alone. These collective data, therefore, provide powerful support for some type of Golgi assembly process occurring within the cell periphery during nocodazole treatment. Central Golgi stacks do not simply break apart and diffuse to peripheral sites.

The above results underscore the highly dynamic nature of the Golgi complex revealed from studies with agents and conditions that cause it to disassemble and reassemble (including BFA, okadaic acid, IQ, and overexpression of ELP1 or mutant Rab 1a) (Lippincott-Schwartz *et al.*, 1990; Lucocq *et al.*, 1991; Hsu *et al.*, 1992; Takizawa *et al.*, 1993; Wilson *et al.*, 1994) and from studies examining the distribution of Golgi enzymes during mitosis (Lucocq and Warren, 1987; Lucocq *et al.*, 1987). It is of considerable interest, therefore, that the number of Golgi fragments that we report during nocodazole treatment (on average 250 per HeLa cell) is the same number Warren and colleagues found during mitosis in HeLa cells using quantitative electron microscopy (Lucocq *et al.*, 1989). Although this similarity may be a coincidence, the fact that many mitotic Golgi clusters were found located next to vesicle budding sites of the ER (Lucocq *et al.*, 1989), suggests an underlying similarity in the process by which Golgi membrane redistributes to peripheral sites during nocodazole treatment and during mitosis.

Given a model for Golgi dispersal during microtubule disruption involving reassembly of Golgi elements at peripheral ER exit sites, how might Golgi membrane components redistribute to these sites? At least two distinct pathways can be envisioned. One involves cytoplasmic diffusion of budded Golgi vesicles to "stacking templates" or "Golgi-organizing centers," which have dispersed during microtubule depolymerization (Turner and Tartakoff, 1989). Alternatively, Golgi membrane enroute to peripheral sites could move through existing membrane structures, like the ER (Saraste and Svensson, 1991; Saraste and Kuismanen, 1992), which extend peripherally throughout the cytoplasm even during nocodazole treatment (Terasaki, 1986). Both of these models are consistent with previous observations on Golgi fragmentation after microtubule disruption, which found that fragmentation is sensitive to energy depletion and membrane traffic perturbants (Turner and Tartakoff, 1991; Table 1), and that rudimentary Golgi formations appear at peripheral sites before central Golgi structures are affected (Busson-Mabillot *et al.*, 1982; Pavelka and Ellinger, 1983). Our observations that ERGIC-53 moves through the ER before accumulating in peripheral fragments during nocodazole treatment (Figure 3), and that Golgi reassembly at peripheral ER sites during nocodazole treatment occurs whether Golgi enzymes are redistributed from centrosomal stacks or from the ER (during BFA washout), however, favor the latter of these models. This led us to investigate the effect of microtubule disruption on the membrane transport pathways connecting the ER and Golgi complex and its potential role in Golgi fragmentation.

Differential Effects of Microtubule Disruption on Anterograde and Retrograde Traffic and Its Role in Golgi Fragmentation

The most common thinking regarding the role of microtubules in ER/Golgi trafficking is that retrograde traffic is dependent on microtubules (Lippincott-Schwartz *et al.*, 1990), while for anterograde traffic microtubules are unnecessary, because microtubule disruption has, in many instances, no effect on secretory transport (Rogalski *et al.*, 1984; Van De Moortele *et al.*, 1993). Our results using quantitative assays to measure anterograde and retrograde traffic operating between the ER and Golgi demonstrated the opposite of this thinking. Retrograde transport was found to be only slightly inhibited by microtubule disruption under all conditions. The effect of microtubule depolymerization on anterograde transport, by contrast, varied depending on the localization of the Golgi complex. Specifically, after early times of nocodazole treatment, anterograde transport of membrane from peripheral ER exit sites into the central Golgi region was completely blocked. Under these conditions, processing of VSV G was significantly reduced compared with control cells. Upon prolonged exposure of cells to nocodazole, once Golgi enzymes redistributed to ER exit sites, the kinetics of VSV G processing became the same as in cells that had never been exposed to the drug.

The above results indicate that microtubules provide transport tracks between the ER and Golgi complex when these compartments are segregated from each other in the cytoplasm. Only after Golgi membrane redistributes to peripheral ER exit sites (as occurs after extended nocodazole treatment) is this microtubule requirement overridden. Thus, Golgi fragmentation is fundamental for ensuring a continuous flow of membrane and content through the secretory pathway during microtubule depolymerization. Upon reestablishing secretory flow from the ER to the Golgi in this manner, transport from dispersed Golgi sites to the cell surface, as shown by Rogalski and Singer (1984) occurs efficiently, but is no longer directed to specific regions of the cell surface. This interpretation offers a reasonable explanation to the conflicting data regarding the role of microtubules in secretion, where some studies have shown no effect of microtubule disruption (Rogalski *et al.*, 1984; Van De Moortele *et al.*, 1993), while others have found significant effects (Redman *et al.*, 1978; Boyd *et al.*, 1982; Breitfield *et al.*, 1990; Gilbert *et al.*, 1991; Rennison *et al.*, 1992). It also supports studies of Saraste and Svensson (1991) that suggested that ER-to-Golgi transport intermediates use microtubules to translocate into the Golgi region.

The finding in this study that microtubule disruption has differential effects on antergrade and retrograde trafficking pathways is significant because this phenomenon has major consequences for membrane components that cycle between the ER and Golgi complex. Specifically, cycling membrane components will accumulate in peripheral structures near ER exit sites after microtubule disruption, because retrograde transport into the ER is only slightly affected, while translocation of peripheral pre-Golgi intermediates into the centrosomal region (where the Golgi usually resides) is blocked under these conditions. This effect of microtubule disruption on membrane cycling between the ER and Golgi was documented for ERGIC-53 in Figure 3, where redistribution of ERGIC-53 from central Golgi structures to peripheral sites occurred within 10–30 min of nocodazole treatment. Because Golgi enzymes redistribute to the same peripheral sites as ERGIC-53 during nocodazole treatment, albeit at a slower rate, it is possible, as depicted in the model shown in Figure 11, that Golgi enzymes slowly flux through the same ER/Golgi pathways as ERGIC-53, and over time accumulate in membrane structures at peripheral ER exit sites due to the failure of these structures to cluster toward the microtubule-organizing center in the absence of microtubules. Consistent with this possibility, inhibitors of retrograde traffic blocked the redistribution of both ERGIC-53 and Golgi enzymes to peripheral sites during nocodazole treatment (Table 1). Moreover, functional Golgi mini-stacks enriched in Golgi enzymes and ERGIC-53 at peripheral ER exit sites were generated during nocodazole treatment whether Golgi enzymes and ERGIC-53 were initially localized to Golgi cisternae near the centrosome, or to the ER before BFA washout (Figure 5).

Extent of Retrograde Traffic by Golgi Enzymes

The above model suggests that the underlying cause of Golgi dispersal during microtubule disruption is a block of the anterograde pathway carrying membranes from peripheral ER exit sites into the centrosomal region of the cell. This implies that the majority of membrane components of the Golgi complex are continually cycling between the ER and Golgi complex at some finite rate and that it is only the requirement for microtubules in anterograde transport that allow us to visualize Golgi fragments during nocodazole treatment. This explanation of Golgi dispersal is reasonable in light of recent data revealing the highly dynamic nature of the Golgi complex (Lucocq *et al.*, 1991; Pelham, 1991; Klausner *et al.*, 1992; Takizawa *et al.*, 1993) and the extent of retrograde membrane traffic (Hsu *et al.*, 1991; Jackson *et al.*, 1993; Tang *et al.*, 1993; Alcade *et al.*, 1994; Lippincott-Schwartz *et al.*, 1995). At present, however, there is no direct evidence that Golgi enzymes normally follow a retrograde pathway, because Golgi enzyme activity is not normally detected within

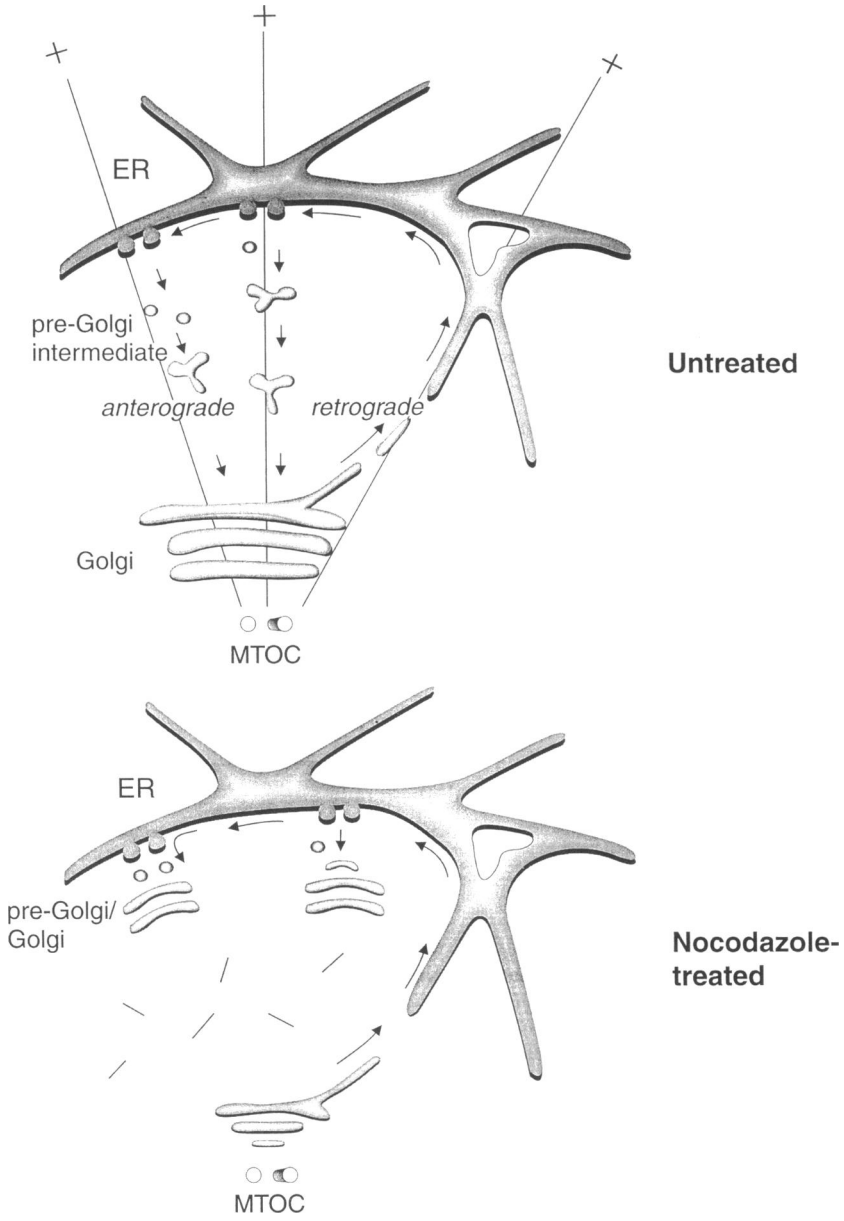

Figure 11. Model for Golgi dispersal during microtubule depolymerization. In untreated cells, Golgi resident proteins would slowly flux through the same ER/Golgi membrane cycling pathways followed by rapidly cycling molecules like ERGIC-53. These molecules follow a retrograde pathway into the ER where they diffuse throughout the network of ER membranes before returning to the Golgi complex along the anterograde pathway. Because retrograde traffic is only slightly inhibited by microtubule disruption, while anterograde transport of peripheral pre-Golgi intermediates into the centrosomal region is blocked, ERGIC-53, as well as Golgi enzymes, would accumulate at ER exit sites upon microtubule disruption. Regeneration of Golgi stacks over time in these peripheral sites would reestablish secretory flow from the ER to the Golgi and result in "Golgi fragmentation."

the ER (Brands *et al.*, 1985; Persson *et al.*, 1992). Nevertheless, it is possible that Golgi enzymes spend only short periods of time passing through the ER, and therefore are difficult to detect there.

In summary, our collective data all point to a model of Golgi fragmentation where recycling Golgi membranes accumulate at peripheral ER exit sites as a consequence of the inability of membranes at these sites to cluster into the centrosomal region in the absence of microtubules. De novo formation of small Golgi stacks at these peripheral sites would reestablish secretory flow from the ER into the Golgi complex and result in the Golgi dispersal phenomenon. This explanation of Golgi dispersal during microtuble disruption predicts unexpectedly heavy retrograde traffic of Golgi enzymes to ER exit sites. It has important implications, therefore, for our understanding of Golgi membrane dynamics and its relationship to microtubule-faciliated ER/Golgi membrane transport pathways.

ACKNOWLEDGMENTS

We are very grateful to Lydia Yuan for her help with electron microscopy. We also thank Drs. Richard Klausner, Juan Bonifacino, Julie Donaldson, Harish Radhakrishna, Mickey Marks, and Mardee

Delahunty for review of the manuscript and for their many valuable scientific discussions.

REFERENCES

Alcade, J., Egea, G., and Sandoval, I.V. (1994). gp74, a membrane glycoprotein of the *cis*-Golgi network that cycles through the endoplasmic reticulum and the intermediate compartment. J. Cell Biol. *124*, 649–665.

Beams, H.W., and Kessel, R.G. (1968). The Golgi apparatus: structure and function. Annu. Rev. Cytol. *23*, 209–276.

Bergmann, J.E. (1989). Using temperature-sensitive mutants of VSV to study membrane protein biogenesis. Methods Cell Biol. *32*, 85–110.

Boyd, A.E., Bolton, W.E., and Brinkley, B.R. (1982). Microtubules and beta cell function: effects of colchicine on microtubules and insulin secretory activity in vitro by mouse beta cells. J. Cell Biol. *92*, 425–434.

Brands R., *et al.* (1985). Retention of membrane proteins by the endoplasmic reticulum. J. Cell Biol. *101*, 1724–1732.

Breitfeld, P.P., McKinnon, W.C., and Mostov, K.E. (1990). Effect of nocodazole on vesicular traffic to the apical and basolateral surfaces of polarized MDCK cells. J. Cell Biol. *111*, 2365–2373.

Busson-Mabillot, S., Chambaut-Guerin, A.-M., Ovtracht, L., Muller, P., and Rossignol, B. (1982). Microtubules and protein secretion in rat lacrimal glands: localization of short-term effects of colchicine on the secretory process. J. Cell Biol. *95*, 105–118.

Cole, N.B., and Lippincott-Schwartz, J. (1995). Organization of organelles and membrane traffic by microtubules. Curr. Opin. Cell Biol. *7*, 55–64.

De Silva, A., Balch, W.E., and Helenius, A. (1990). Quality control in the endoplasmic reticulum: folding and misfolding of vesicular stomatis virus G protein in cells and in vitro. J. Cell Biol. *111*, 857–866.

Farquhar, M.G. (1991). Protein traffic through the Golgi complex. In: Intracellular Trafficking of Proteins, New York, NY: Cambridge University Press, 431–471.

Farquhar, M.G., and Palade, G.E. (1981). The Golgi apparatus (complex)-(1954–1981): from artifact to center stage. J. Cell Biol. *91*, 77–103.

Gilbert, T., Bivac, A.L., Quaroni, A., and Rodriquez-Boulan, E. (1991). Microtubular organization and its involvement in the biogenetic pathways of plasma membrane proteins in Caco-2 intestinal epithelial cells. J. Cell Biol. *113*, 275–288.

Griffiths, G., Fuller, S.D., Hollinshead, M., Pfeiffer, S., and Simons, K. (1989). The dynamic nature of the Golgi complex. J. Cell Biol. *108*, 277–297.

Griffiths, G., Pepperkok, R., Krijnse Locker, J., and Kreis, T.E. (1995). Immunocytochemical localization of β-COP to the ER-Golgi boundary and the TGN. J. Cell Sci. *108*, 2839–2856.

Hauri, H-P., and Schweizer, A. (1992). The endoplasmic reticulum: Golgi intermediate compartment. Curr. Opin. Cell Biol. *4*, 600–608.

Ho, W.C., Allan, V.J., van Meer, G., Berger, E.G., and Kreis, T.E. (1989). Reclustering of scattered Golgi elements occurs along microtubules. Eur. J. Cell Biol. *8*, 250–263.

Hsu, V.W., Shah, N., and Klausner, R.D. (1992). A brefeldin A-like phenotype is induced by the overexpression of a human ERD-2-like protein, ELP-1. Cell *69*, 625–635.

Hsu, V.W., Yuan, L.C., Nuchtern, J.G., Lippincott-Schwartz, J., Hammerling, G.J., and Klausner, R.D. (1991). A recycling pathway between the endoplasmic reticulum and the Golgi apparatus for retention of unassembled MHC class I molecules. Nature *352*, 441–444.

Jackson, M.R., Nilsson, T., and Peterson, P.A. (1993). Retrieval of transmembrane proteins to the endoplasmic reticulum. J. Cell Biol. *121*, 317–333.

Klausner, R.D., Donaldson, J.G., and Lippincott-Schwartz, J. (1992). Brefeldin A: insights into the control of membrane traffic and organelle structure. J. Cell Biol. *116*, 1071–1080.

Laemmli, U.K. (1970). Cleavage of structural proteins during the assembly of the head of bacteriophage T4. Nature *227*, 680–685.

Lippincott-Schwartz, J., Cole, N.B., Marotta, A., Conrad, P.A., and Bloom, G.S. (1995). Kinesin is the motor for microtubule-mediated Golgi-to-ER membrane traffic. J. Cell Biol. *128*, 293–306.

Lippincott-Schwartz, J., Donaldson, J.G., Schweizer, A., Berger, E.G., Hauri, H.P., Yuan, L.C., and Klausner, R.D. (1990). Microtubule-dependent retrograde transport of proteins into the ER in the presence of brefeldin A suggests an ER recycling pathway. Cell *60*, 821–836.

Luby-Phelps, K. (1994). Physical properties of the cytoplasm. Curr. Opin. Cell Biol. *6*, 3–9.

Lucocq, J.M., Berger, E.G., and Warren, G. (1989). Mitotic Golgi fragments in HeLa cells and their role in the reassembly pathway. J. Cell Biol. *109*, 463–474.

Lucocq, J.M., Pryde, J.G., Berger, E.G., and Warren, G. (1987). A mitotic form of the Golgi apparatus in HeLa cells. J. Cell Biol. *104*, 865–874.

Lucocq, J.M., and Warren, G. (1987). Fragmentation and partitioning of the Golgi apparatus during mitosis in HeLa cells. EMBO J. *6*, 3239–3246.

Lucocq, J., Warren, G., and Pryde, J. (1991). Okadaic acid induces Golgi apparatus fragmentation and arrest of intracellular transport. J. Cell Sci. *100*, 753–759.

McLean, I.W., and Nakane, P.K. (1974). Periodate-lysine-paraformaldehyde fixation: a new fixative for immunoelectron microscopy. J. Histochem. Cytochem. *22*, 1077–1083.

Mellman, I., and Simons, K. (1992). The Golgi complex: in vitro veritas? Cell *68*, 829–840.

Mizuno, M., and Singer, S.J. (1994). A possible role for stable microtubules in intracellular transport from the endoplasmic reticulum to the Golgi apparatus. J. Cell Sci. *107*, 1321–1331.

Pavelka, M., and Ellinger, A. (1983). Effect of colchicine on the Golgi complex of rat pancreatic acinar cells. J. Cell Biol. *97*, 737–748.

Pelham, H.R. (1991). Recycling of proteins between the endoplasmic reticulum and Golgi complex. Curr. Opin. Cell Biol. *3*, 585–591.

Penman, S. (1995). Rethinking cell structure. Proc. Natl. Acad. Sci. USA *92*, 5251–5257.

Pepperkok, R.J., Scheel, J., Horstmann, H., Hauri, H.-P., Griffiths, G., and Kreis, T.E. (1993). βCOP is essential for biosynthetic membrane transport from the endoplasmic reticulum to the Golgi in vitro. J. Cell Biol. *122*, 1155–1168.

Persson, R., Schnell, C.R., Haken Borg, L.A., and Fries, E. (1992). Accumulation of Golgi-processed secretory protein in an organelle of high density upon reduction of ATP concentration in rat hepatocytes. J. Biol. Chem. *267*, 2760–2766.

Peter, F., Plutner, H., Zhu, H., Kries, T.E., and Balch, W.E. (1993). Beta-COP is essential for transport of protein from the endoplasmic reticulum to the Golgi in vitro. J. Cell Biol. *122*, 1155–1167.

Plutner, H., Davidson, H.W., Saraste, J., and Balch, W.E. (1992). Morphological analysis of protein transport from the ER to Golgi

membranes in digitonin-permeabilized cells: role of the p58-containing compartment. J. Cell Biol. *119*, 1097–1116.

Pryer, N.K., Wuestehube, L.J., and Schekman, R. (1992). Vesicle-mediated protein sorting. Annu. Rev. Biochem. *61*, 471–516.

Rambourg, A., and Clermont, Y. (1990). Three-dimensional electron microscopy: structure of the Golgi apparatus. Eur. J. Cell Biol. *51*, 189–200.

Redman, C.M., Banerjee, D., Manning, C., Huang, C.Y., and Green, K. (1978). In vivo effect of colchicine on hepatic protein synthesis and on the conversion of proalbumin to serum albumin. J. Cell Biol. *77*, 400–416.

Rennison, M.E., Handel, S.E., Wilde, C.J., and Burgoyne, R.D. (1992). Investigation of the role of microtubules in protein secretion from lactating mouse mammary epithelial cells. J. Cell Sci. *102*, 239–247.

Rogalski, A.A., Bergmann, J.E., and Singer, S.J. (1984). Effect of microtubule assembly status on the intracellular processing and surface expression of an integral protein of the plasma membrane. J. Cell Biol. *99*, 1101–1109.

Rogalski, A.A., and Singer, S.J. (1984). Associations of elements of the Golgi apparatus with microtubules. J. Cell Biol. *99*, 1092–1100.

Rothman, J.E. (1994). Mechanisms of intracellular protein. Nature *372*, 555–563.

Rothman, J.E., and Orci, L. (1992). Molecular dissection of the secretory pathway. Nature *355*, 409–415.

Saraste, J., and Kuismanen, E. (1984). Pre- and post-Golgi vacuoles operate in the transport of Semliki Forest virus membrane glycoproteins to the cell surface. Cell *38*, 535–549.

Saraste, J., and Kuismanen, E. (1992). Pathways of protein sorting and membrane traffic between the rough endoplasmic reticulum and the Golgi complex. Semin. Cell Biol. *3*, 343–355.

Saraste, J., and Svensson, K. (1991). Distribution of the intermediate elements operating in ER to Golgi transport. J. Cell Sci. *100*, 415–430.

Schweizer, A., Fransen, J.A., Matter, K., Kreis, T.E., Ginsel, L., and Hauri, H.P. (1990). Identification of an intermediate compartment involved in protein transport from endoplasmic reticulum to Golgi apparatus. Eur. J. Cell Biol. *53*, 185–196.

Schweizer, A., Fransen, J.A.M., Bachi, T., Ginsel, L., and Hauri, H.-P. (1988). Identification, by a monoclonal antibody, of a 53-kD protein associated with a tubulo-vesicular compartment at the *cis*-side of the Golgi apparatus. J. Cell Biol. *107*, 1643-1653.

Takizawa, P.A., Yucel, J.K., Veit, B., Faulkner, D.J., Deerinck, T., Soto, G., Ellisman, M., and Malhotra, V. (1993). Complete vesiculation of Golgi membranes and inhibition of protein transport by a novel sea sponge metabolite, ilimaquinone. Cell *73*, 1079–1090.

Tang, B.L., Wong, S.H., Qi, X., Low, S.H., and Hong, W. (1993). Molecular cloning, characterization, subcellular localization and dynamics of p23, the mammalian KDEL receptor. J. Cell Biol. *120*, 325–338.

Terasaki, M., Chen, L.B., and Fujiwara, K. (1986). Microtubules and the endoplasmic reticulum are highly interdependent structures. J. Cell Biol. *103*, 1557–1568.

Thyberg, J., and Moskalewski, S. (1985). Microtubules and the organization of the Golgi complex. Exp. Cell Res. *159*, 1–6.

Turner, J.R., and Tartakoff, A.M. (1989). The response of the Golgi complex to microtubule alterations: the roles of metabolic energy and membrane traffic in Golgi complex organization. J. Cell Biol. *109*, 2081–2088.

Van De Moortele, S., Picart, R., Tixier-Vidal, A., and Tougard, C. (1993). Nocodazole and taxol affect compartments but not secretory activity of GH3B6 prolactin cells. Eur. J. Cell Biol. *60*, 217–227.

Warren, G. (1993). Membrane partitioning during cell division. Annu. Rev. Biochem. *62*, 323–348.

Wehland, J., Henkart, M., Klausner, R.D., and Sandoval, I.V. (1983). Role of microtubules in the distribution of the Golgi apparatus: effect of taxol and microinjected anti-α-tubulin antibodies. Proc. Natl. Acad. Sci. USA *80*, 4286–4290.

Wilson, B.S., Nuoffer, C., Meinkoth, J.L., McCaffery, M., Feramisco, J.R., Balch, W.E., and Farquhar, M.G. (1994). A Rab1 mutant affecting guanine nucleotide exchange promotes disassembly of the Golgi apparatus. J. Cell Biol. *125*, 557–571.

Yuan, L.C., Barriocanal, J.G., Bonifacino, J.S., and Sandoval, I.V. (1987). Two integral membrane proteins located in the *cis*-middle and *trans* part of the Golgi system acquire sialylated N-linked carbohydrates and display different turnovers and sensitivity to cAMP-dependent phosphorylation. J. Cell Biol. *105*, 215–227.